Oriented Nonspherical Atoms in Crystals Deduced from X-Ray Scattering Data

by **Lance L. Miller**, **Robert A. Jacobson**, and **Klaus Ruedenberg***

Ames Laboratory, U.S. Department of Energy, Iowa State University, Ames, Iowa 50011-3020, USA

and

Jier Niu and **W. H. Eugen Schwarz**

Theoretical Chemistry Group, The University, D-57068 Siegen, Germany

Dedicated to *Edgar Heilbronner* in honor of his 80th birthday with the authors' cordial good wishes

A crystallographic pro-molecule/pro-crystal model is described that goes beyond the standard reference model, which explicitly contains only numerically determined atomic positions and thermal vibrational smearings, while leaving all other information lumped together in a so-called deformation density. The new model includes further explicit parameters that identify valence-orbital orientations and occupancies of degenerate or near-degenerate atomic ground states in crystals. A method is described for extracting this additional information as well from X-ray data by least-mean-squares refinements. It is applied to the experimental data sets of three organic molecules: 9-(*tert*-butyl)anthracene, tetrafluoroterephthalonitrile, and 1,2,3-triazine. The electronic structure inferences are discussed.

1. Introduction. – **1.1.** ***Atoms in Molecules.*** On the most elementary level, matter consists of coupled quantum fields and, in the quantum-chemical regime, it is described by electrically coupled *nuclear and electronic wave functions.* The interactions between these fundamental constituents are, however, of such a nature that an eminently successful description of all phenomena encountered over the last two hundred years within the realm of experimental chemistry has been achieved by the *granular model of atoms in molecules* [1]. In the later stages of this development, the determination of the atomic structures of crystals by X-ray diffraction has played a prominent role [2]. Since this experimental technique essentially provides an account of the electron density [3][4], the resulting modeling of crystals in terms of atoms reduces to an interpretation of the *observed* electron densities of crystals in terms of atomic electron densities derived, in some manner, from *quantum theoretically calculated ground-state wave functions of free atoms.*

The approach universally taken in this endeavor is to approximate the total electron density as a superposition of atomic densities. This is because it would be unrealistic to try to deduce superpositions of atomic *wave amplitudes* (the approach that proves successful in quantum-chemical calculations) from experimental *densities* of the available accuracy (see, *e.g.*, [5–8])[1]).

Nonetheless, molecular and crystal electron densities *cannot* be obtained as straightforward superpositions of atomic *ground-state* densities and the differences

[1]) A somewhat different approach is described in [9–12].

between the former and the latter, howsoever constructed, have come to be called *difference densities*. (Some authors also use the term 'deformation density', but we will not do so since we wish to reserve the concept of 'deformation' for a specific and more precisely defined purpose to be discussed presently.) Difference densities are manifestations of the 'chemical forces' acting between the atoms, and it is clearly in the spirit of the atomic model to look for conceptual models that can furnish interpretations of difference densities by relating them to the variety of bonding patterns that so enchant chemists. Particularly gratifying, at least in the eyes of the present authors, would be model concepts bearing some relationship to quantum-mechanical conclusions regarding chemical bonding.

Within the crystallographic context, such a superposition of atomic densities is called a *promolecule* or *procrystal reference*. The conventional standard for promolecules is based on *spherically averaged* and configuration-states-averaged self-consistent-field-density distributions of the free atoms, superposed at their crystallographic positions and vibrationally smeared. The success of this simple vibrating-ball model can be attributed to four reasons[2]): *i*) The model already recovers all gross features of the actual electron density; *ii*) the model has yielded a wealth of basic structural information that has proven elucidative for the understanding of many chemical properties; *iii*) the agreement to use such a simple model has provided an unambiguous practical reference basis for the comparison of the results from different research groups; *iv*) until fairly recently, experimental limitations made it difficult to routinely determine X-ray data with an accuracy that would warrant an in-depth exploration of more elaborate atom models. However, with the advent of more powerful diffraction techniques, differences between experimental electron densities in crystals and superpositions of atomic ground-state densities have become accessible to a much higher degree of accuracy so that the optimal choice of the promolecule model deserves re-examination.

1.2. ***Orientation and Deformation of Atoms.*** In this search, it would seem desirable to define the atomic constituents in such a manner that they retain their individuality and the character of the free atoms as much as possible. With such an aim in mind, we focus attention on the fact that, *for atoms with degenerate (or near-degenerate) ground states*, as is common for open p-, d-, and f-valence shells, *any arbitrary superposition of the degenerate (or near-degenerate) partner functions is an equally valid ground-state wave function or, more generally, ground-state ensemble density operator*. (For instance, the superposition of all degenerate functions with equal weights is spherically symmetric.) The corresponding ground-state densities can, therefore, assume many different shapes, all of which are isoenergetic in the free atom. We shall call these kinds of density modifications *orientations* of the ground-state density. Since they can occur without energetic resistance in the free atoms, such orientations can be caused even by minuscule long-range forces. Now, quantum-chemical calculations show beyond any dispute that, whatever the definition of the atomic constituents, they rarely are

---

[2]) In support of such a promolecule choice, it has also been argued that all free-atom densities are intrinsically always spherical. This intuitive *a priori* assertion is, however, at variance with basic quantum theory, as will be discussed in *Chapt. 1.2*.

spherically symmetric in a molecule[3]). In view of the aforementioned orientational flexibility of degenerate ground states, it seems, therefore, reasonable to construct promolecules from ground-state densities that are *oriented in the sense* just defined so as to approach the local molecular densities as closely as possible. This uniquely specifies the atomic-ground-states ensemble density, in addition to the positional distribution. It is found that the difference density between such an optimally oriented promolecule and the actual molecule (crystal) is always comparatively *small* whereas the density changes that are induced by *arbitrary* selections of *alternative* ground-state orientations, including the spherical choice, can become quite large [13–15]. The *optimal local orientational ground-state adaptation* of any atom in the molecule is, therefore, in the spirit of preserving the characteristics of the free atoms while adapting them to the local bonding situation.

In the context of such a model (and excluding thermal vibrations for the moment), the 'chemical forces' are seen as causing two modifications of the atomic (quasi)degenerate ground-state ensemble densities after the latter have been simply superposed at their molecular equilibrium positions, namely: *i*) the individual atomic ground states are oriented and *ii*) the total density is further deformed by an additional the addition of the difference density. The latter embodies *deformations* that are *genuinely interatomic* in the sense that *they cannot be recovered by any (intra-atomically isoenergetic) reorientations of the atomic ground states.* They comprise density modifications that, in quantum-chemical treatments, are associated with atomic promotions, orbital polarizations and hybridizations, orbital overlaps, interatomic interferences, *Pauli* exclusion effects, *etc.* We find it, therefore, expedient *i*) *not* to use the term 'deformation' to describe the ground-state *orientations*, and *ii*) to use the term *deformation difference density* (DDD) for the difference density defined with reference to the oriented atoms[4]). While the DDDs contain significant bonding information, the most consequential effects of the binding forces are the establishment of the atomic positions in the molecule *and* the orientations of the ground-state atoms [16][17].

The deviation of an oriented ground-state density from sphericity can be effectively exhibited by forming the difference between the oriented and the spherically averaged ground-state densities. We may call this difference the *orientational difference density* (ODD). In the case of open p-shells, often has a predominantly quadrupolar character around the atomic positions as noted, *e.g.*, by *Bader* [18]. It is apparent that the conventional difference density, which we shall call the *total difference density* (TDD = crystal density minus spherically averaged atomic densities) can be expressed as the sum of the orientational and the deformational difference densities introduced here: TDD = ODD + DDD. The conceptual resolution of TDD implied by this identity offers certain insights. Not only can the ODD terms for atoms with degenerate ground states be considerably larger than the DDD terms, but they are also less sensitive to errors in the experimental analysis [14][19]. Furthermore, the same atom may exhibit

---

[3]) Here and in the following, 'molecule' also means 'crystal'.

[4]) This is a slight change compared to the nomenclature we used in previous papers where we called this quantity the 'chemical deformation density'.

quite different ground-state orientations under different coordination conditions, leading to a wide variety in ODD and, hence, TDD shapes. By contrast, much more regularity is found to exist for the DDD features [13–15]. At the same time, the orientational terms are described by only a small number of parameters that have transparent physical meanings, whereas the reduction of the information embedded in the DDD terms to a small parameter set would appear to be very difficult in most cases. It seems, therefore, infelicitous from an interpretative as well as an information-theoretical point of view to mix the density changes described by these two kinds of terms.

It may be clarifying to compare the approach of the optimal ground-state orientation *i*) with the standard HO treatment (*i.e.*, the determination of the locations and vibrations of the contributing *spherical* atomic densities by highly weighting the high-order scattering data) as well as *ii*) with the multipole refinement (which follows the HO refinement with the addition of multipole expansions at the atomic positions as an effective way of deforming the atomic densities *beyond* the orientational changes discussed so that their superposition *completely* recovers the observed electron density). Such a comparison is exhibited in *Table 1*.

Table 1. *Comparison of Refinement Methods*

	Standard HO refinement	Present approach	Multipole refinement
Refined parameters	Structural parameters	Structural parameters and atomic orientations	Structural parameters and total deformation density
Remainder	TDD and errors 'large' R value	DDD and errors 'medium' R value	Residual errors 'small' R value
Interpretable quantities	*i*) Structural parameters *ii*) Features overlaid in the TDD map	*i*) Structural parameters *ii*) Orientation parameters *iii*) Deformation difference density	*i*) Structural parameters *ii*) Features overlaid in the TDD map *iii*) Valence-shell multipoles

In view of what has been said, the introduction of oriented promolecules deserves exploration as a worthwhile further development of the model of atoms in molecules. Within our model, three aspects are thus distinguished in molecule formation: *i*) the positioning of the atomic cores at the equilibrium positions and their vibrational smearing; *ii*) the orientation of the atomic ground-state valence shells according to directions most suitable for the specific chemical bonds to be formed; and *iii*) an additional redistribution of electronic charge associated with the establishment of these bonds. In crystals, the electron density may be further deformed by intermolecular forces, librations, *etc*. Such a conceptual differentiation is appealing from a quantum-chemical perspective provided that the local adaptation of the oriented promolecules can be accomplished by a general, unambiguous, and nonarbitrary definition.

Certain caveats should be understood. For example, it would not be a simple matter to associate energy increments with the aforementioned three aspects, and they would depend upon whether the orientations of the atoms are envisioned to take place before

or after they are put in their molecular positions[5]). Furthermore, any conceptual decomposition of the kind discussed represents an analysis of the state of the molecule *at the equilibrium geometry* and is only very indirectly related to mechanistic questions of bond-formation kinetics – a statement that is, of course, equally valid for the geometrical structure itself.

1.3. ***Implementation.*** It is the objective of the present investigation to show that the framework described can be filled with quantitative content by tying it to experimental information derived from X-ray diffraction through a nonarbitrary procedure. The first step is the determination of the equilibrium positions of the atoms as well as their vibrations by appropriate conventional methods. The second step is, then, the determination of the optimally adapted oriented atomic ground states. To this end, an appropriate valence-orbital set must be selected from the (near) degenerate ground-state ensemble of each atom. The oriented atomic ground-state density of such an atom can then be expressed in the diagonal form ($\Sigma_n N_n \phi_n^2$), where the ϕ_n are orthonormal linear combinations of the valence orbitals and the N_n are the corresponding occupation numbers. These are the parameters that describe the ground-state density orientations, and their determination will be discussed below. The third step is then the calculation of difference densities.

The fundamental aspects of such an approach have been described in a series of papers [13–15][20–34]. Two nonarbitrary methods were formulated for the optimal orientational adaptation of atomic ground states to local molecule/crystal densities. One method consists of minimizing the mean-square deviation between the oriented promolecule density and the actual density of the molecule/crystal *in direct space*, and this approach has been quantitatively applied to a number of theoretically calculated individual molecules [15][22][31][34]. Its application to crystal densities obtained from multipolar X-ray refinements is currently being studied. The second method, which is the subject of this paper, consists of minimizing the mean-square deviation *in k-space* between the scattering intensities derived from the oriented promolecule and the actual crystal-diffraction intensities [13][33]. The implementation was first worked out by *Miller* [13] and subsequently further pursued by *Nin* [14]. It has been applied to several experimental data sets [13][14][34][35]. The explicit implementation has been worked out by *Miller* [13], and it is the basis for the present investigation. A gratifying consistency is found between the results deduced from the two approaches.

2. Theory. – **2.1.** ***Basic Equations.*** The promolecule [36] used in this work is formed from a superposition of atoms that, in turn, are superpositions of spherical cores, and of oriented ground-state valence orbitals weighted by their occupation numbers N_{an} [34][37]. The basic equations have been derived in [13] and [33]. The electron-density expression for the a^{th} atom (*sans* thermal and atom site occupancy corrections) is

---

[5]) In this context, it is of some interest that the electrostatic Coulombic interaction energy between the oriented ground-state atoms, superposed at the quantum-mechanical equilibrium positions, roughly parallels the quantum-mechanical interaction energy. This is presumably so because *i*) according to the virial theorem, the electrostatic Coulomb and exchange-correlation energy at the nuclear equilibrium geometry is equal to twice the bond energy, and *ii*) the former can roughly be approximated by the Coulomb energy of the promolecular density [16][17]. This Coulombic model will not *yield* the equilibrium geometry however.

$$\rho_a(\mathbf{r}) = \Sigma_{\mu\nu}\, \chi_\mu(\mathbf{r})\, \chi_\nu(\mathbf{r})\, P_{a\mu\nu} \tag{1a}$$

$$P_{a\mu\nu} = \Sigma_n N_{an} V_{a\mu n} V_{avn} \tag{1b}$$

where N_{an} are the eigenvalues (orbital occupancies) and V_{avn} the eigenvectors (orbital orientations/shapes) of the atomic one-electron density matrix $\mathbf{P}_a$. *They embody the orientational information of the atomic densities.* The subscript μ represents the quantum number set (nlm) of the μ^{th} atomic reference orbital $\chi_{a\mu}(\mathbf{r}) = R_{nl}(\mathrm{r})\, Y_{lm}(\theta,\phi)$. The spherical harmonics Y_{lm} refer to an orthogonal reference frame, which, in the case of nonorthogonal unit cells, is related to the lattice vectors by standard formulas.

In reciprocal space, the experimental crystal-structure factors $F^{\text{obs}}(\mathbf{k})$ are approximated by a linear combination of atomic scattering factors $f_a(\mathbf{k})$

$$F^{\text{obs}}(\mathbf{k}) \approx F(\mathbf{k}) = s\, x(\mathbf{k})\, \Sigma_a\, m_a\, T_a(\mathbf{k})\, f_a(\mathbf{k})\, \exp(i\mathbf{k}\cdot\mathbf{r}_a) \tag{2}$$

where $\mathbf{r}_a$ are the atomic positions in the unit cell, and s is the overall scale factor. The factor $x(\mathbf{k})$ is an empirical extinction correction [38–42]. The factors m_a are the atom-site-occupancy multipliers, and $T_a(\mathbf{k})$ are the usual temperature factors [43][44]. *Eqn. 2* may be separated into real and imaginary parts, $F = F' + iF''$, *viz.* for each atom:

$$F'_a(\mathbf{k}) = s\, x(\mathbf{k})\, m_a\, T_a(\mathbf{k})\, [f_a^g(\mathbf{k})\, \cos(\mathbf{k}\cdot\mathbf{r}_a) - f_a^u(\mathbf{k})\, \sin(\mathbf{k}\cdot\mathbf{r}_a)] \tag{3a}$$

$$F''_a(\mathbf{k}) = s\, x(\mathbf{k})\, m_a\, T_a(\mathbf{k})\, [f_a^u(\mathbf{k})\, \cos(\mathbf{k}\cdot\mathbf{r}_a) + f_a^g(\mathbf{k})\, \sin(\mathbf{k}\cdot\mathbf{r}_a)]. \tag{3b}$$

The atomic scattering factor

$$f_a(\mathbf{k}) = \Sigma_n N_{an} f_{ann}(\mathbf{k}) \tag{4a}$$

is the sum of the orbital occupancies N_{an} times the oriented orbital-scattering factors

$$f_{amn}(\mathbf{k}) = \Sigma_{\mu\nu}\, V_{a\mu m} f_{a\mu\nu}(\mathbf{k})\, V_{avn}. \tag{4b}$$

The standard orbital scattering functions $f_{a\mu\nu}(\mathbf{k})$, for atomic orbitals $|a\mu\rangle$ *and* $|a\nu\rangle$, are

$$f_{a\mu\nu}(\mathbf{k}) = \Sigma_L\, \langle a\mu\,|\, j_L(k)\,|\, a\nu\rangle\, Z_L(\mu,\nu)/4\pi \tag{5}$$

where $\langle a\mu\,|\, j_L\,|\, a\nu\rangle$ and $Z_L(\mu,\nu)$ are the *Fourier* transforms of the radial and angular parts of the wave function products, respectively [45]. The functions $Z_L(\mu,\nu)$ for s-, p-, and d-shells were computed on the basis of spherical *Bessel* functions from [46] and are given in *Table 2*. The SCF radial functions used to calculate the $\langle a\mu\,|\, j_L\,|\, a\nu\rangle$ were from *Raffenetti* [47], and *Raffenetti* and *Ruedenberg* [48]. The Y_{LM} functions in k-space [49] occurring in *Table 2*, are given with the proper phases in *Table 3*. The integrals [50] denoted in *Table 2* as V_L for $M = |m_\mu| + |m_\nu|$ and as W_L for $M = |m_\mu| - |m_\nu|$ are given in *Table 4* for the L-range $[|l_\mu - l_\nu|, (l_\mu + l_\nu)]$. Each of the 'f' functions given in

Table 2. *The* $Z_L(\mu, \nu)$*Functions*

m_1 [a])	m_2 [a])	$Z_L(\mu, \nu)$		
0	0	$V_L(l_1 0, l_2 0)Y_{L0}$		
m	0	$V_L(l_1 m, l_2 0)Y_{Lm}$		
0	m	$V_L(l_1 0, l_2 m)Y_{Lm}$		
$-m$	0	$V_L(l_1 m, l_2 0)Y_{L(-m)}$		
0	$-m$	$V_L(l_1 0, l_2 m)Y_{L(-m)}$		
m	m	$1/\sqrt{2}V_L(l_1 m, l_2 m)Y_{L(2m)}$	+	$W_L(l_1 m, l_2 m)Y_{L0}$
$-m$	m	$1/\sqrt{2}V_L(l_1 m, l_2 m)Y_{L(-2m)}$		
m	$-m$	$1/\sqrt{2}V_L(l_1 m, l_2 m)Y_{L(-2m)}$		
$-m$	$-m$	$-1\sqrt{2}V_L(l_1 m, l_2 m)Y_{L(2m)}$	+	$W_L(l_1 m, l_2 m)Y_{L0}$
m_1	m_2	$1/\sqrt{2}V_L(l_1 m_1, l_2 m_2)Y_{L(m_1+m_2)}$		$+1/\sqrt{2}W_L(l_1 m_1, l_2 m_2)Y_{L\lvert m_1-m_2\rvert}$
$-m_1$	m_2	$1/\sqrt{2}V_L(l_1 m_1, l_2 m_2)Y_{L(-m_1-m_2)}$		$+1/\sqrt{2}W_L(l_1 m_1, l_2 m_2)Y_{L(-\lvert m_1-m_2\rvert)}\ sign(m_1-m_2)$
m_1	$-m_2$	$1/\sqrt{2}V_L(l_1 m_1, l_2 m_2)Y_{L(-m_1-m_2)}$		$-1/\sqrt{2}W_L(l_1 m_1, l_2 m_2)Y_{L(-\lvert m_1-m_2\rvert)}\ sign(m_1-m_2)$
$-m_1$	$-m_2$	$-1/\sqrt{2}V_L(l_1 m_1, l_2 m_2)Y_{L(m_1+m_2)}$		$+1/\sqrt{2}W_L(l_1 m_1, l_2 m_2)Y_{L\lvert m_1-m_2\rvert}$

[a]) m_i is a positive number, $-m_i$ is a negative number.

Table 3. *The* $Y_{LM}(h, k, l)$ *Functions*

L M	$Y_{LM}(h, k, l)$	L M	$Y_{LM}(h, k, l)$
0 0	1	2-2	$\sqrt{15}\ hk/\lvert\vec{h}\rvert^2$
		2-1	$\sqrt{15}\ kl/\lvert\vec{h}\rvert^2$
1-1	$\sqrt{3}\ k/\lvert\vec{h}\rvert$	2 0	$\sqrt{5/4}\ (3l^2-\lvert\vec{h}\rvert^2)/\lvert\vec{h}\rvert^2$
1 0	$\sqrt{3}\ l/\lvert\vec{h}\rvert$	2 1	$\sqrt{15}\ h\ l/\lvert\vec{h}\rvert^2$
1 1	$\sqrt{3}h/\lvert\vec{h}\rvert$	2 2	$\sqrt{15/4}\ (h^2-k^2)/\lvert\vec{h}\rvert^2$
3-3	$\sqrt{35/8}k(3h^2-k^2)/\lvert\vec{h}\rvert^3$	4-4	$\sqrt{315/4}\ hk(h^2-k^2)/\lvert\vec{h}\rvert^4$
3-2	$\sqrt{105}\ hkl/\lvert\vec{h}\rvert^3$	4-3	$\sqrt{315/8}\ kl(3h^2-k^2)/\lvert\vec{h}\rvert^4$
3-1	$\sqrt{21/8}k(5l^2-\lvert\vec{h}\rvert^2)/\lvert\vec{h}\rvert^3$	4-2	$\sqrt{45/4}\ hk(7l^2-\lvert\vec{h}\rvert^2)/\lvert\vec{h}\rvert^4$
3 0	$\sqrt{7/4}\ l(5l^2-3\lvert\vec{h}\rvert^2)/\lvert\vec{h}\rvert^3$	4-1	$\sqrt{45/8}\ kl(7l^2-3\lvert\vec{h}\rvert^2)/\lvert\vec{h}\rvert^4$
3 1	$\sqrt{21/8}\ h(5l^2-\lvert\vec{h}\rvert^2)/\lvert\vec{h}\rvert^3$	4 0	$3/8\ (35l^4-30l^2\lvert\vec{h}\rvert^2+3\lvert\vec{h}\rvert^4)/\lvert\vec{h}\rvert^4$
3 2	$\sqrt{105/4}\ l(h^2-k^2)/\lvert\vec{h}\rvert^3$	4 1	$\sqrt{45/8}\ hl(7l^2-3\lvert\vec{h}\rvert^2)/\lvert\vec{h}\rvert^4$
3 3	$\sqrt{35/8}\ h(h^2-3k^2)/\lvert\vec{h}\rvert^3$	4 2	$\sqrt{45/16}\ (h^2-k^2)(7l^2-\lvert\vec{h}\rvert^2)/\lvert\vec{h}\rvert^4$
		4 3	$\sqrt{315/8}\ hl(h^2-3k^2)/\lvert\vec{h}\rvert^4$
		4 4	$\sqrt{315/64}\ (h^4-6h^2k^2+k^4)/\lvert\vec{h}\rvert^4$

Eqns. 4 and *5* have either gerade or ungerade character depending on whether $l_\mu + l_\nu$ is even or odd[6]).

The unitary spectral representation matrix $\mathbf{V}_a$ diagonalizes the electron density matrix, $\mathbf{P}_a = \mathbf{V}_a\mathbf{N}_a\mathbf{V}_a^+$, which may be used to rewrite *Eqns. 4* as

$$f_a(\mathbf{k}) = \Sigma_{\mu,\nu} P_{a\mu\nu} f_{a\mu\nu}(\mathbf{k}). \tag{6}$$

Since the filled (core) shells are assumed to be isotropic, with $\mathbf{V}_a = \mathbf{1}$ and $N_a = 2$, *Eqn. 4* is explicitly needed only for the open valence shell(s). Anomalous dispersion, being mainly a core electron phenomenon, is added in the standard fashion only to the core electron shells' scattering factors.

---

[6]) The odd case will not occur for the orientation of degenerate ground states except when nearly degenerate states of different parity are mixed, *e.g.*, in the case of valence s → p promotion.

Table 4. *The* V_L *and* W_L *Functions*

AO Pair		AO Pair	
ss	$V_0(00, 00) = 1$	sd	$V_2(00, 20) = 1$
			$V_2(00, 21) = 1$
sp	$V_1(00, 10) = 1$		$V_2(00, 22) = 1$
	$V_1(00, 11) = 1$		
		dd	$V_0(20, 20) = 1$
pp	$V_0(10, 10) = 1$		$V_2(20, 20) = \sqrt{20/49}$
	$V_2(10, 10) = \sqrt{4/5}$		$V_4(20, 20) = 6/7$
	$V_2(11, 10) = \sqrt{3/5}$		$V_2(21, 20) = \sqrt{5/49}$
	$V_2(11, 11) = \sqrt{6/5}$		$V_4(21, 21) = \sqrt{30/49}$
	$W_0(11, 11) = 1$		$W_0(21, 21) = 1$
	$W_2(11, 11) = -\sqrt{1/5}$		$V_2(21, 21) = \sqrt{30/49}$
			$W_2(21, 21) = \sqrt{5/49}$
pd	$V_1(10, 20) = \sqrt{4/5}$		$V_4(21, 21) = \sqrt{40/49}$
	$V_3(10, 20) = \sqrt{27/35}$		$W_4(21, 21) = -4/7$
	$V_1(10, 21) = \sqrt{3/5}$		$V_2(22, 20) = -\sqrt{20/49}$
	$V_3(10, 21) = \sqrt{24/35}$		$V_4(22, 20) = \sqrt{15/49}$
	$V_3(10, 22) = \sqrt{3/7}$		$W_2(22, 21) = \sqrt{30/49}$
	$V_1(11, 20) = -\sqrt{1/5}$		$V_4(22, 21) = \sqrt{35/49}$
	$V_3(11, 20) = \sqrt{18/35}$		$W_4(22, 21) = -\sqrt{5/49}$
	$W_1(11, 21) = \sqrt{3/5}$		$W_0(22, 22) = 1$
	$V_3(11, 21) = \sqrt{6/7}$		$W_2(22, 22) = -\sqrt{20/49}$
	$W_3(11, 21) = -\sqrt{9/35}$		$V_4(22, 22) = \sqrt{10/7}$
	$W_1(11, 22) = \sqrt{6/5}$		$W_4(22,22) = 1/7$
	$V_3(11,22) = \sqrt{9/7}$		
	$W_3(11, 22) = -\sqrt{3/35}$		

The promolecule/procrystal reference may thus be assembled in reciprocal space, from atoms with densities determined by the electron density matrices $\mathbf{P} = \mathbf{VNV}^+$, by using the equations given above, the look-up *Tables 2–4*, and the tabulated radial functions $\langle a\mu \,|\, j_L \,|\, a\nu \rangle$ [13][45].

Our atomic form factors refer to ground *states* (*e.g.*, ^{3}P in carbon) and not to ground *configuration averages* (*e.g.*, ^{3}P, ^{1}D, ^{1}S carbon), as do those in the *International Tables* [45]. In carbon, for example, the difference Δf is less than 0.03 for $sin(\theta)/\lambda < 0.2$ Å^{-1}. Correspondingly, the expectation value $\langle 2p \,|\, r \,|\, 2p \rangle$ is $3.74a_0$ for the ground-state and $3.89a_0$ for the ground-configuration average.

2.2. *Least Squares.* The weighted-least-squares refinement of the promolecule's variables [13][33] is accomplished through iterative refinement of variables ν, u by $\Delta\nu$, Δu determined by the normal *Newton-Gauss* equations [51–53]

$$\Sigma_k\, \omega_k\, \Sigma_r\, [\partial\,|\,F(\mathbf{k})\,|\,/\partial\nu]\, [\partial\,|\,F(\mathbf{k})\,|\,/\partial\nu]\, \Delta u = \Sigma_k\, \omega_k\, [\,|\,F^{\mathrm{obs}}(\mathbf{k})\,|\, -\, |\,F(\mathbf{k})\,|\,]\, \partial\,|\,F(\mathbf{k})\,|\,/\partial\nu, \tag{7a}$$

or, in matrix notation

$$\Sigma_r A_{\nu u} \Delta u = B_\nu, \tag{7b}$$

where F^{obs} and F are the experimental and model structure factors, and, according to *Eqn. 3*,

$$\partial\,|\,F(\mathbf{k})\,|\,/\partial v = [\partial F'(\mathbf{k})/\partial v]\,\cos(\alpha_k) + [\partial F''(\mathbf{k})/\partial v]\,\sin(\alpha_k) \tag{8a}$$

with

$$\cos(\alpha_k) = F'(\mathbf{k})/\,|\,F(\mathbf{k})\,|\,,\ \sin(\alpha_k) = F''(\mathbf{k})/\,|\,F(\mathbf{k})\,|\,. \tag{8b}$$

The various derivatives are collected in *Table 5*. A modification of the standard procedure is introduced for the orientation coefficients $V_{a\mu m}$. To guarantee the orthogonality of the matrix $\mathbf{V}_a$ in *Eqns. 1b* and *4b*, an antisymmetric matrix $\Delta\mathbf{t}_a$ is introduced. One determines the shifts Δt_{amn}, $(m<n)$ and then uses the following relationship to obtain an improved, exactly orthogonal $\mathbf{V}_a$ in the next iteration step $i+1$:

$$\mathbf{V}_a^{i+1} = \mathbf{V}_a^i(\mathbf{I} - \Delta\mathbf{t}_a/2)^{-1}(\mathbf{I} + \Delta\mathbf{t}_a/2). \tag{9}$$

Table 5. *Derivatives of the Structure Factors*

Parameter v	$\partial F'/\partial v$
s	F'/s
$\mathrm{m_a}$	F'_a/m_a
x_{ai}	$-2\pi\,h_i\,F''_a$
U_a	$-8\pi\sin^2(\theta)/\lambda^2\,F'_a$
$U_{aij}\,(i\cdot j)$	$(\delta_{ij}-2)\,h_i\,h_j\,a_i^*\,a_j^*\,F'_a$
N_{an}	$s\,m_a\,T_a(k)\,[f^{\mathrm{g}}_{an}\cos(k\cdot r_a) - f^{\mathrm{u}}_{an}(k)\sin(k\cdot r_a)]$
$t_{amn}\,(m<n)$	$2(N_{an}-N_{am})\,s\,m_a\,T_a(k)\,f^{\mathrm{g}}_{amn}\cos(k\cdot r_a)$
$V_{a\mu m}$	$s\,m_a\,T_a\,(k)\,2\,N_{am}\,[\Sigma_\nu\,f^{\mathrm{g}}_{a\mu\nu}\,V_{avm}\cos(k\cdot r_a) - \Sigma_\nu\,f^{\mathrm{u}}_{a\mu\nu}\,V_{avm}\sin(k\cdot r_{\mathrm{a}})]$
Parameter v	$\partial F''/\partial v$
s	F''/s
m_a	F''_a/m_a
x_{ai}	$2\pi\,h_i\,F'_a$
U_a	$-8\pi\sin^2(\theta)/\lambda^2\,F''_a$
$U_{aij}\,(i\cdot j)$	$(\delta_{ij}-2)\,h_i\,h_j\,a_i^*\,a_j^*\,F''_a$
N_{an}	$s\,m_a\,T_a(k)\,[f^{\mathrm{g}}_{an}\sin(k\cdot r_a) + f^{\mathrm{u}}_{an}\cos(k\cdot r_a)]$
$t_{amn}\,(m<n)$	$2(N_{an}-N_{am})\,s\,m_a\,T_a(k)\,f^{\mathrm{u}}_{amn}\cos(k\cdot r_a)$
$V_{a\mu m}$	$s\,m_a\,T_a\,(k)\,2\,N_{am}\,[\Sigma_\nu\,f^{\mathrm{g}}_{a\mu\nu}\,V_{avm}\sin(k\cdot r_a) + \Sigma_\nu\,f^{\mathrm{u}}_{a\mu\nu}\,V_{avm}\cos(k\cdot r_{\mathrm{a}})]$

Other constraints and restraints, which may be needed to keep parameters from having nonphysical or symmetry-breaking values, may be handled by standard practices [13][51–54]. The orbital occupancies present a typical problem. According to the *Pauli* principle, they are restrained to lie in the interval [0, 2]. To realize atomic neutrality, the total number of electrons on an atom must be fixed. *Lagrange* multipliers λ_a may be used to maintain the relation

$$\Sigma_m \Delta N_{am} = 0 \tag{10}$$

for each atom a. For the simple case of a single atom, one minimizes

$$G = \Sigma_k\,\omega_k\,(\Delta F_k)^2\ -\ 2\lambda_a\Sigma_m\Delta N_{am} \tag{11a}$$

where ΔF means ($|F^{obs}| - |F|$), leading to

$$\Sigma_{km}\,\omega_k\,[\partial^2|F(\mathbf{k})|/\partial N_{an}\partial N_{am}]\,\Delta N_{am}=\Sigma_k\,\omega_k\,\Delta F_k\,[\partial|F(\mathbf{k})|/\partial N_{an}]+\lambda_a \qquad (11b)$$

or in matrix form

$$\Sigma_m\,A_{nm}\,\Delta N_m=B_n+\lambda_a. \qquad (11c)$$

Instead of solving *Eqns. 10* and *11c* simultaneously, one may also apply a two-step partitioning procedure. One solves *Eqn. 11c* formally for ΔN_m and inserts it in *Eqn. 10:*

$$\Sigma_{mn}\,(A^{-1})_{mn}\,B_n+\lambda_a\Sigma_{mn}\,(A^{-1})_{mn}=0 \qquad (11d)$$

from which λ_a is obtained. *Eqn. 11c* is then solved for the occupancy-shift vector ΔN*:*

$$\Delta N_m=\Sigma_n\,(A^{-1})_{mn}\,B_n+\lambda_a\Sigma_n\,(A^{-1})_{mn}. \qquad (11e)$$

In principle, the constraint of atomic neutrality may be relaxed to that of molecular or unit-cell neutrality. However, the fitting of partial atomic changes to molecular and crystal densities frequently yields rather small charge values even for strongly polar compounds (*e.g.*, [55–58]). We shall therefore not pursue this avenue here.

Additional constraints on the angular part of the wave function arise when oriented atoms lie on crystallographic symmetry elements. In handling these, one must introduce constraints on the $\Delta\mathbf{t}$ in *Eqn. 9*. As an example, consider an atom with valence p-orbitals lying on a mirror plane normal to the *c*-axis of an orthorhombic space group. One of its symmetry-adapted orbitals, ψ_3, must be perpendicular to the mirror plane, the other two orbitals lie in the mirror plane. In this case all elements of the matrix **V** may be expressed as a function of a single rotation parameter θ:

	ψ_1	ψ_2	ψ_3
p_x	$\cos\theta$	$-\sin\theta$	0
p_y	$\sin\theta$	$\cos\theta$	0
p_z	0	0	1

(12a)

That is, only the submatrix Δt_{xy} may be nonzero and the derivatives of each **V** matrix elements w.r.t. θ are needed to form the normal equations. Alternatively, the symmetry constraint can be maintained by introducing the two side conditions

$$\Delta t_{xz}=0,\ \Delta t_{yz}=0 \qquad (12b)$$

and adding the corresponding Lagrangian term

$$-2\lambda_{xz}\Delta t_{xz}\ -\ 2\lambda_{yz}\Delta t_{yz} \qquad (12c)$$

to the function *G* of *Eqn. 11a*.

Using appropriately redefined **V** matrices, one may also incorporate predefined orbitals based on chemical intuition into the promolecule. Such a choice may, however, result in a non-ground-state promolecule reference of known energy that goes beyond the premises of the present work.

2.3. *Difference Densities.* A difference-density distribution $\delta\rho = \rho - \rho_{\text{reference}}$ is obtained by computing the *Fourier* transform of the corresponding difference in *k*-space, *viz.*

$$\delta\rho(\mathbf{r}) = (1/V_{\text{cell}})\Sigma_k \Delta F(\mathbf{k}) \exp(-i\mathbf{k}\cdot\mathbf{r}) \tag{13a}$$

with the overall standard deviation of

$$\sigma(\rho) = (1/V_{\text{cell}})(\Sigma_k[\Delta F(\mathbf{k})^2])^{1/2}. \tag{13b}$$

The signal-to-noise ratio is increased by using only reflections for which $|F^{obs}(\mathbf{k})| > n.\sigma(F^{obs}(\mathbf{k}))$, where $\sigma(F^{obs}(\mathbf{k}))$ is the standard deviation of a reflection [41]. Although *k* truncation effects are no longer a severe problem in *Eqn. 13b*, the highest *k* values in *Eqn. 13a* contribute more *Fourier* truncation ripples and noise than they contribute to physical-density features [59][60]. Therefore, we usually cut the *Fourier* summation at $k_{Max} = \sin(\theta_{Max})/\lambda$ *ca.* 1 Å^{-1}.

Three kinds of difference densities are created and examined:

$$\begin{aligned}\text{TDD} &= \rho(\text{experiment}) - \rho(\text{spherically averaged promolecule})\\ &= \text{total difference density}\end{aligned} \tag{14}$$

$$\begin{aligned}\text{DDD} &= \rho(\text{experiment}) - \rho(\text{oriented promolecule})\\ &= \text{deformation difference density}\end{aligned} \tag{15}$$

$$\begin{aligned}\text{ODD} &= \rho(\text{oriented promolecule}) - \rho(\text{spherically averaged promolecule})\\ &= \text{orientation difference density}\end{aligned} \tag{16}$$

[32–34]. They are related by

$$\text{TDD} = \text{ODD} + \text{DDD} \tag{17}$$

as was already mentioned in the third paragraph in *Chapt. 1.2*. It has been shown previously that the magnitude of ODD can vary enormously whereas that of DDD always stays within rather small bounds [15]. Consequently, the contribution of ODD to TDD can vary from very little to nearly all of it [22][21][15][30][32]. The resolution of *Eqn. 17* can, therefore, be helpful in understanding the origin of the TDD features.

An apt interpretation of the present analysis is provided by the following perturbation-theoretical model: the *zeroth order* effect of the bonding interactions is the positioning of the atoms at their equilibrium positions, *i.e.*, the establishment of bond lengths and bond angles as well as their vibrational parameters. *Moreover*, if a free-atom ground-state is degenerate, as is common for open p-, d-, and f-valence shells, then zeroth-order degenerate perturbation theory *also* requires this ground-state to adapt to the bonding situation by appropriate *orientation*. *In addition*, the bonding forces cause genuine (*i.e.*, nonorientational) *deformations* of the electron density *in higher order*. They are embodied in DDD and offer further insights into the bonding characteristics.

3. Implementation. – 3.1. *Procedure of Application.* Our study begins with an absorption-corrected high-resolution data set and the approximate atomic positions. For the high STOL ($\equiv\sin(\theta)/\lambda$) values, mainly the localized core electrons contribute to the intensity; whereas both the core and the valence electrons contribute to the low-order data with 2s and 2p electrons (of second-row atoms B to F), giving quite similar contributions [59][60]. Since bonding causes some localized density features in the valence region and some overall contraction of the valence shell, while thermal motions extend the core density, the core-valence separation in *k*-space becomes less sharp in molecules than for free atoms at rest. Calculations of the valence density of several organic crystals using various upper limits of STOL showed indeed that the resultant average peak heights of selected bond centers, considered as a function of the upper STOL limit, reached the high-order plateau for larger k-values than is the case in the corresponding free atoms. We concluded that STOL values up to $k = 0.7$ to 0.9 Å^{-1} contribute to the valence density of second row atoms.

The *core-type parameters* (coordinates and thermal parameters of the non-hydrogen atoms with core electrons) and the overall-scale factor, are reasonably well determined [61] by standard least-squares refinement against the data above this STOL cutoff (the HO data). Next, the remaining *valence-type parameters* (coordinates and thermal parameters of hydrogen; valence-orbital occupations, orientations, and shapes of open valence shells) and the extinction parameters are determined by least-squares refinement against all data. Determination of the core-type parameters from the HO data alone is not only necessary for obtaining good values for atomic positions but it is also essential to prevent a mixing of the asymmetries of the thermal vibrations (in the core parameters) with the asymmetries of the valence-shell orientations (in the valence parameters). The parameters describing these two types of non-sphericities become strongly correlated when they are *simultaneously* determined by an all-data refinement leading to significant errors. Our procedure yields valence occupations in reasonable agreement with those from quantum-theoretical calculations on individual molecules which are unadulterated by thermal vibrations and/or experimental noise.

Given a proper choice of the STOL cutoff, no great changes of scale and thermal parameters happen upon simultaneous refinements of the core- and valence-type parameters. In such refinements, the latter two types of parameters change significantly less than their sigmas. Depending upon the quality of the data set and the type of atom, the sigmas of the orbital occupancies typically lie between 0.01e and 0.1e. Directions of orbitals with significantly different occupancies are typically determined within a few degrees. However, when two orbital occupancies differ from each other by less than $\Delta N = 0.1$, then the two corresponding directions become computationally indeterminate (typically by (several degrees $\times \Delta N^{-1}$)) with respect to each other, which, of course, is a reflection of the physical freedom existing in this case.

For the H-atoms, we use either reliable parameters from the literature (*e.g.*, neutron diffraction or multipole refinement), or we refine the hydrogen parameters using *Stewart*'s [62] modified form factor in a first step and then expand the A–H bond length to the standard A–H bond length, *i.e.*, by *ca.* 10%. Then, we use the free-atom hydrogen form factor to refine the orbital parameters of the other atoms and to generate the density maps. This empirical adjustment should be kept in mind in the ensuing interpretations. The change of the A–H bond lengths from the X-ray values to

realistic values is accompanied by occupation-number changes of up to 0.05e and by orientational changes of several degrees.

3.2. *Presentation of Results.* Conventional promolecules are typically represented using ORTEP [63] exhibiting the positional and vibrational information. In addition to these parameters, our promolecule models contain the valence-orbital orientations and occupancies (and shapes in case of d- and f-AOs). To present all three types of information, *positional*, *vibrational*, and *valence orbital*, simultaneously in a single figure is impractical. A clearer visualization is achieved by using two pictures, a conventional one for the positional and vibrational information, and another one exhibiting the positional and valence-shell information. *Fig. 1* illustrates the latter technique as applied to the molecule 1,2,3-triazine (experimental data from *Angermund* [38]).

In *Fig. 1*, *a*, the standard information on atom positions and thermal vibrations is depicted in the usual manner by vibrational ellipsoids placed at the molecule's nuclear centers. Harmonic normal-vibrations in three-dimensional space are specified by three directional and three amplitude parameters per atom, which are represented by the directions and lengths of the ellipsoids' principal axes. In *Fig. 1*, *b*, the same graphical technique is also used to represent the three directions and three occupancies of the three p-orbitals of an open-p-shell atom. Anharmonic vibrations as well as orbital orientations involving sp or sd hybrids, or d shells can be represented by higher-order ORTEP surfaces [3][4].

Another orbital representation (*Fig. 1*, *c*) utilizes sticks and balls. The size of the balls represents the orbital occupancies and the stick directions are the orbital directions. Alternatively, we may represent the p-orbitals by rods using SCHAKAL [64], as shown in *Fig. 1, d*. Here the occupancy/orientation of each orbital is represented by the length/orientation of its rod. Finally, the valence AO information can also be displayed through contour maps, as will be mentioned below in connection with *Fig. 2*, *c*, at the end of this section or, simply, by numerical tables.

Each of *Figs. 1*, *b*, *c*, and *d* present the same orbital information. The representation of *Fig. 1, d*, exhibits more clearly the orientation of strongly aspherical atoms. On the other hand, when two or three p-orbital occupancies are very similar, orbital directions lose much of their uniqueness, and the representation of *Fig. 1*, *b*, is more appropriate.

The remaining information, *i.e.*, the information contained in the experimental data set but not our model, is then represented graphically by the deformation difference density plot of DDD in two or three dimensions.

As an example, *Fig. 2*, *a*, shows a two-dimensional TDD map of 1,2,3-triazine in the molecular plane, where the spherically averaged atom reference has been subtracted from the observed density. Note that the TDD shows much left-right asymmetry, whereas the bonding situation in the molecule is fairly symmetric even in the crystal.

Fig. 2, *b* shows a DDD map, prepared by subtracting the oriented atom promolecule from the observed density. The DDD shows less detail than the TDD. The 'missing' information has been transferred into the valence-shell parameters. Note the approximate left-right symmetry in this figure, corresponding to the approximately symmetric *intra*molecular bonding forces.

Fig. 2, *c*, displays a map of the orientational difference density $\mathrm{ODD} = \rho(\text{oriented reference atoms}) - \rho(\text{spherical reference atoms}) = \mathrm{TDD} - \mathrm{DDD}$, which manifestly

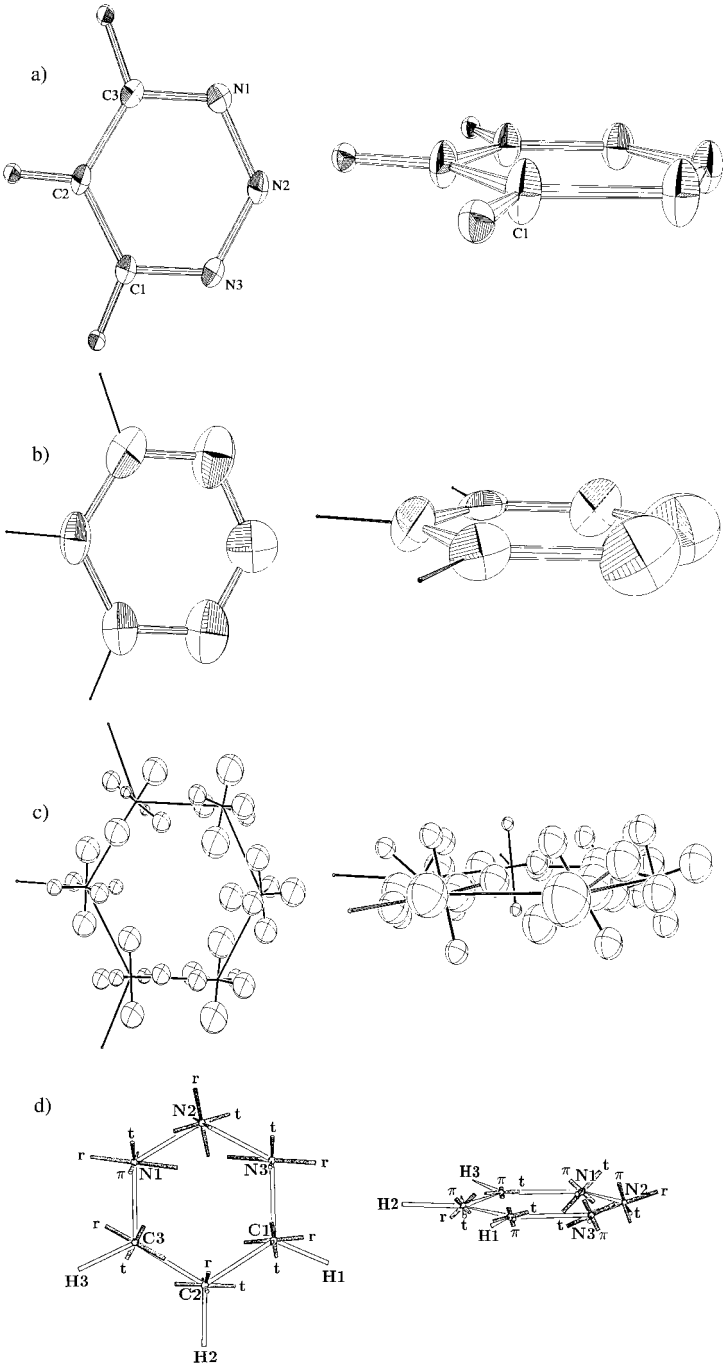

Fig. 1. *Graphical representation of numerical information on 1,2,3-triazine. a*) Standard ellipsoid representation of positional and vibrational information. Representations of orbital occupancies and orientations by *b*) ellipsoids; *c*) pseudo-atoms; and *d*) rods (see text).

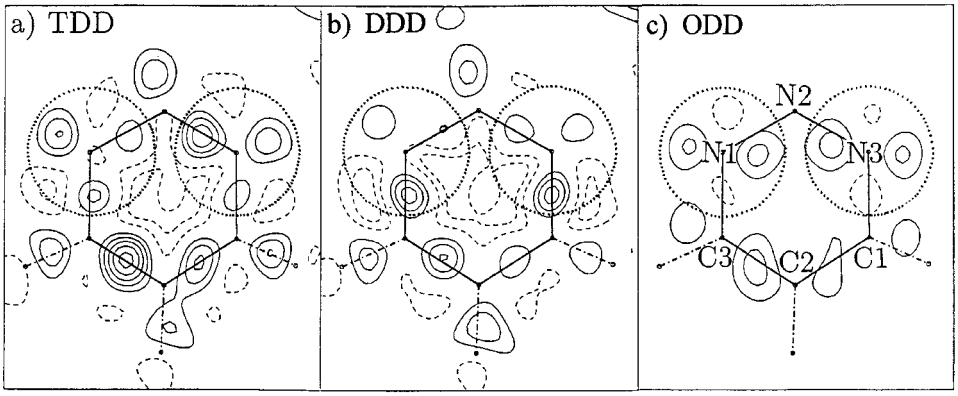

Fig. 2. *Electron-density maps of 1,2,3-triazine in the molecular plane. a*) TDD map, ρ(molecule) – ρ(spherical atoms); *b*) DDD map, ρ(molecule) – ρ(oriented atoms); *c*) ODD map, ρ(oriented atoms) – ρ(spherical atoms). Values of $\Delta\rho$-contour lines are $n \times 0.1 e/Å^3$, where $n = \pm 1, \pm 2, \ldots$; dashed lines indicate negative $\Delta\rho$ values. Dotted circles are drawn around N(1) and N(3) to guide the eye (see text).

furnishes a graphical presentation of the information regarding the oriented valence-shell against a spherically averaged atomic background. It is seen that the oriented nonspherical population of an open p-shell will give quadrupolar character to the independent atoms in the molecule, which is most apparent in the molecular plane of *Fig. 2,c*, for the N(1) and N(3) atoms. (The carbon quadrupoles are more apparent in a vertical plane). The left-right asymmetry of this feature (the orientations of N(1) and N(2) deviate by $\pm 9°$ from left-right symmetry) may result from *inter*molecular packing effects in the crystal and/or from systematic and statistical errors of the experiments.

It is apparent that the features of TDD (*Fig. 2,a*) are the result of lumping together two kinds of features with fairly different characteristics, namely: *i*) the strongly quadrupolar features of ODD (*Fig. 2,c*) due to the valence-shell *orientations*, and *ii*) the trigonal *deformations* inherent in the DDD (*Fig. 2,b*), which are manifestly related to the trigonal bonding coordination.

4. Applications. – In this section, we report the results of using the described approach to analyze the experimental diffraction data of three crystals, *viz.*, 9-(*tert*-butyl)anthracene (TBA), tetrafluoroterephthalonitrile (TFT), and 1,2,3-triazine (TA). To discuss the relation of such analyses to questions of chemical bonding, we also report complementary results obtained, *for the corresponding isolated molecules*, by fitting promolecule densities in direct space to the densities of *quantum mechanically calculated electronic wave functions* of the individual molecules. (The latter were obtained by SCF calculations with double-zeta plus single polarization basis sets). We shall often refer to *these* promolecules and difference densities as the '*theoretical*' quantities while denoting the analogous quantities deduced from the crystallographic analyses as the '*experimental*' promolecules and difference densities. *A close similarity will be shown to exist between the corresponding experimental and theoretical quantities*, and this agreement will prove valuable in illuminating the experimental results, since theoretical promolecules can be analyzed and understood in as much detail as desired. The latter analyses explain in particular certain systematic

differences between the atomic-orbital *occupancies* found by fitting *densities* through superposition of atomic densities and *Mulliken*-type atomic-orbital *populations* deduced from molecular electronic *wave functions.*

4.1. *9-(*tert*-Butyl)anthracene (TBA).* 4.1.1. *TBA Refinement.* A summary of the crystallographic information for 9-(*tert*-butyl)anthracene (data from [38][65]) is given in *Table 6*. ORTEP Drawings [63] of the TBA promolecule are shown in *Fig. 3*. The $\sin(\theta)/\lambda$ (STOL) cutoff, which separates the high-order (HO) and low-order (LO) data to determine the atomic core parameters independently of the valence deformations, was 0.65 $Å^{-1}$ [13]. The STOL cutoffs are compromises between a value large enough to eliminate all chemical deformation effects on the core parameters and a value small enough to leave a sufficiently large ratio (No. of data/No. of parameters). This cutoff left 2235 HO reflections for the refinement of 163 core-type parameters (non-hydrogen positional and thermal parameters, and the scale factor), which were refined in a first stage, where atomic densities with spherically averaged valence shells were applied in the traditional manner. The results are similar to those reported by the authors of the original measurements.

In the second stage, the 162 valence-type parameters (hydrogen positional and vibrational parameters and orientation valence-shell parameters of non-H-atoms) were refined against all the data. The results of the refinement are given in *Tables 6* and *8*. Subsequent refining of the valence parameters decreased the R_w^I value from 0.028 to 0.024, *i.e.*, by 14%, and the least-squares error (LSE; *i.e.*, physical information, experimental noise, and bias of the model, reflected in the difference density maps) by

Table 6. *Crystal and Data Parameters for 9-(*tert*-Butyl)anthracene (TBA), Tetrafluoroterephthalonitrile (TFT), and 1,2,3-Triazine (TA)*

Reference name	TBA	TFT	TA
Molecular formula	$C_{18}H_{18}$	$C_8N_2F_4$	$N_3C_3H_3$
Crystal system	monoclinic	orthorhombic	triclinic
Space group symbol	$P2_1/c$	*Cmca*	$P\bar{1}$
Lattice parameters			
a [Å]	11.137	7.6848	5.7688
b [Å]	6.8927	9.7350	6.8732
c [Å]	17.792	9.5549	5.6725
α [°]	90	90	110.08(0)
β [°]	107.68(0)	90	113.94(7)
γ [°]	90	90	95.30(2)
Temp.	100 K	98 K	100 K
Radiation	MoK_α	MoK_α	MoK_α
$\sin(\theta)/\lambda$ [min/max, $Å^{-1}$]	0.047/0.855	0.098/1.151	0.08/0.90
Number of reflections	42375	17740	9046
Number after averaging	6805	2387	2187
Number observed ($I > 0$)	4587	2179	2032
Internal agreement[a])	0.049	0.016	0.027
R_ω^I (TDD)	0.028	0.041	0.063
R_ω^I (DDD)	0.024	0.029	0.056
LSE(DDD)/LSE(TDD)[b])	0.83	0.50	0.77

[a]) $R_{Int} = (\Sigma_k |\ \langle I\rangle - I\ |)/(\Sigma_k |\ \langle I\rangle\ |)$. [b]) $\mathrm{LSE} = \Sigma_k\ \omega_k\ (\Delta F_k)^2$.

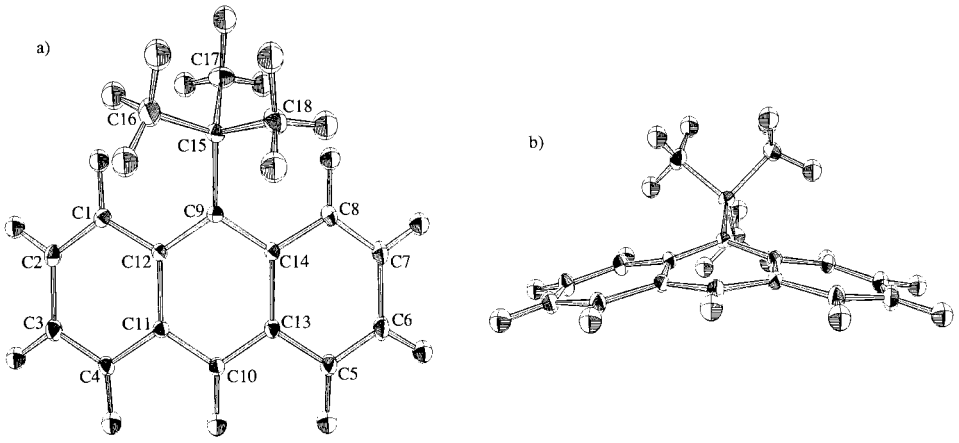

Fig. 3. *Top* (*a*) *and side* (*b*) *views of ellipsoid representation of the C-atoms in 9-(*tert-*butyl)anthracene (TBA) representing core positions and vibrational directions and amplitudes.*

19%. This part of the information has thus been extracted from the TDD and is used to determine the valence parameters.

There is evidence for rotational disorder in the *t*-Bu group. Since rotational disorder was not allowed for in the reference model, the effects will show up as anomalous thermal parameters that are not able to model the rotation correctly. The consequence is that the valence orbitals will be smeared in an artificial manner making their interpretation potentially misleading. For this reason, the Me C-atoms (C(16)–C(18)) will not be discussed further.

4.1.2. *TBA Core Parameters* (*Fig. 3*). From the atomic positions, we obtain the most important information about bonding, namely the bond lengths, bond angles, and dihedral angles. The bond lengths (in Å) are very similar to those in unsubstituted anthracene (AN) [66] and may be interpreted in the conventional manner, *e.g.*, assuming a bond length–bond order correlation (*Table 7*). The standard deviation of the bond lengths is *ca.* 0.001 Å, resulting in $\sigma \approx 0.01$. Only the bonds to C(9), at which the bulky *t*-Bu group is substituted, are expanded (by more than 0.03 Å in comparison to AN) with corresponding angular distortions (visible in *Fig. 3*,*b*). The intermolecular interactions cause very small asymmetric deformations of left and right bond lengths of at most 0.003 Å.

Table 7. *Bond Lengths and Bond Orders for 9-(*tert-*Butyl)anthracene (TBA), Compared to Anthracene (AN)*

Bonds	Bond lengths [Å]		Bond order	
	TBA	AN	TBA	AN
C(1)–C(2), C(3)–C(4), C(5)–C(6), C(7)–C(8)	1.37(1)	1.36(1)	1.7(9)	1.8(5)
C(10)–C(11), C(10)–C(13)	1.39(7)	1.40(1)	1.6(4)	1.6(2)
C(9)–C(12), C(9)–C(14)	1.43(0)	1.40(1)	1.4(6)	1.6(2)
C(2)–C(3), C(6)–C(7)	1.42(5)	1.42(8)	1.4(9)	1.4(8)
C(1)–C(12), C(4)–C(11), C(5)–C(13), C(8)–C(14)	1.43(7)	1.43(4)	1.4(3)	1.4(5)
C(11)–C(12), C(13)–C(14)	1.44(5)	1.43(6)	1.3(9)	1.4(3)

4.1.3. *TBA Valence AO Parameters* (*Figs. 4* and *5,c*). *Table 8* shows the p-orbital occupancies N_i, the valence-shell quadrupole parameter

$$q = N_1 - (N_2 + N_3)/2$$

(where the numbering 1 to 3 is uniquely chosen so that $(N_1 - N_2) \cdot (N_2 - N_3) > 0$ and $|N_1 - N_2| > |N_2 - N_3|$), and the p-AO orientations. All C-atoms have nearly the same standard deviations of $\sigma(\mathrm{N}) \approx 0.07\mathrm{e}$, $\sigma(\mathrm{q}) = 0.1\mathrm{e}$. The local coordinate vectors for the valence orbitals are perpendicular ('*v*'), radially outward ('*r*'), and tangential ('*t*') to the respective rings for atoms C(1) through C(10). For C(11) to C(14), the directions '*r*' and '*t*' are parallel and perpendicular to the cross-bonds. For C(15): '*r*' is radially outward along the C(9)–C(15) vector, and '*t*' lies parallel to the average molecular plane. The promolecule's valence-shell information is presented graphically in *Figs. 4* and *5,c*.

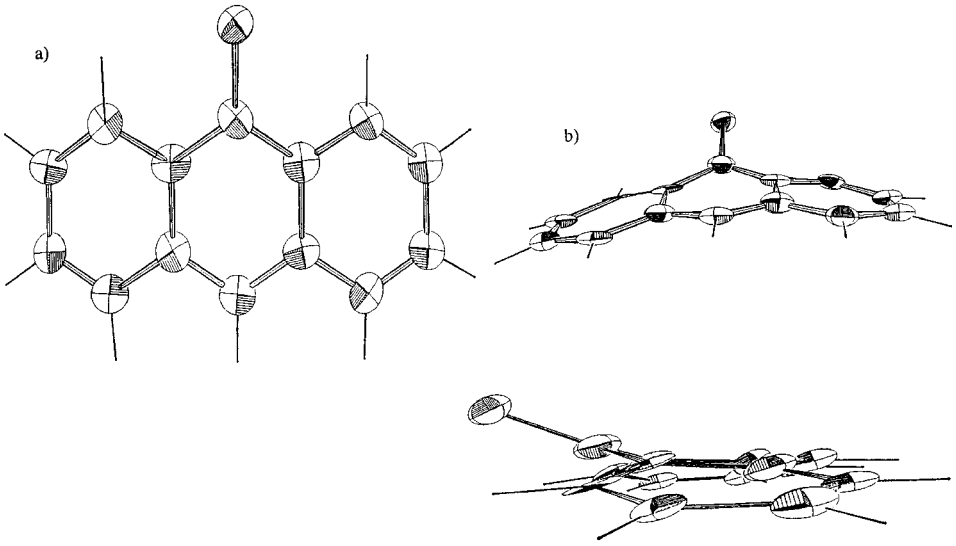

Fig. 4. *Top* (*a*) *and side* (*b*) *views of ellipsoid representation of the C-atoms in TBA representing positions and valence-orbital directions and occupancies.* c) *Representation highlighting common rotation of atoms.*

There is a great deal of similarity among the atoms within the anthracene rings. Each atom has a low occupancy of *ca*. 0.2e in one orbital with a refined orientation approximately normal to the ring. In chemical terms, these are the carbon $2p\pi$ orbitals. The other two p orbitals (both $2p\sigma$) have approximately equal occupancies of 0.9e. The atomic ground-state density determined by the interatomic interactions in the molecule exhibits thus an oblate cylindrical symmetry of the atomic valence shells with an average quadrupole parameter $q \approx 0.7_7$. This oblate valence configuration of all ring atoms best matches the electron density of these aromatic molecules while remaining *intra-atomically* isoenergetic with the spherically averaged atom state. The typical aromatic γ-crystal packing of the molecules [13][65] leads to a rotation of all oblate

Table 8. *Valence-Orbital Parameters for the C-Atoms* C_j *of TBA*. In each column: first entry = occupation N_i of the *i*th p-AO; next three entries = cosines between orbital direction and radial (r), tangential (t), and vertical (v) direction with respect to the rings. π-AO: nearly vertical to the rings; *t*-AO: nearly tangential to the rings, *r*-AO: pointing radially towards the ring center. The value under the C_j is the valence shell quadrupolar parameter $q = N_1 - (N_2 + N_3)/2$. The standard deviations are $\sigma(N) \approx 0.07$, $\sigma(q) \approx 0.01$.

Atom, q		π-AO	*t*-AO	*r*-AO	Atom, q	π-AO	*t*-AO	*r*-AO
C(1)	N_i	0.00	0.97	1.03	C(8)	0.11	0.90	0.99
$q = -1.00$	'*r*'	0.29	0.61	0.73	$q = -0.83$	−0.44	−0.36	0.82
	'*t*'	0.07	0.75	−0.66		0.03	0.91	0.42
	'*v*'	0.95	−0.25	0.17		0.90	−0.21	0.39
C(2)		0.13	0.71	1.16	C(9)	0.25	0.99	0.76
$q = -0.81$		0.08	0.34	0.94	$q = -0.63$	0.36	−0.68	0.64
		0.32	0.88	−0.34		0.10	0.71	0.70
		0.94	−0.33	0.04		0.93	0.19	−0.32
C(3)		0.22	0.95	0.83	C(10)	0.18	0.98	0.84
$q = -0.68$		0.18	0.42	0.89	$q = -0.72$	0.39	0.10	0.91
		0.14	0.88	0.45		−0.02	0.99	−0.10
		0.98	−0.20	−0.10		0.92	−0.02	−0.39
C(4)		0.11	1.07	0.82	C(11)	0.20	0.86	0.94
$q = -0.83$		0.19	0.07	0.98	$q = -0.69$	0.37	−0.45	0.81
		−0.17	0.99	−0.04		−0.18	0.82	0.54
		0.97	0.15	−0.20		0.91	0.34	−0.22
C(5)		0.25	0.70	1.05	C(12)	0.03	1.13	0.84
$q = -.63$		−0.15	−0.67	0.73	$q = -0.95$	0.42	0.05	0.91
		0.04	0.73	0.68		0.08	0.99	−0.10
		0.99	−0.13	0.09		0.91	−0.11	−0.41
C(6)		0.19	0.86	0.95	C(13)	0.25	1.02	0.74
$q = -0.72$		0.26	0.37	0.89	$q = -0.63$	−0.53	0.16	0.83
		0.11	0.91	−0.41		0.06	0.99	−0.14
		0.96	0.21	0.20		0.85	0.03	0.53
C(7)		0.17	0.95	0.88	C(14)	0.11	0.99	0.90
$q = -0.76$		0.04	0.46	0.89	$q = -0.84$	−0.33	−0.09	0.94
		−0.26	0.86	−0.44		−0.09	0.99	0.07
		0.97	0.21	−0.15		0.94	0.06	0.34
C(15)		0.35	0.78	0.86				
$q = -0.46$		−0.76	0.40	0.51				
		0.62	0.69	0.38				
		0.20	−0.60	0.77				

ring atoms out of the ring planes by *ca*. 20° (with $\sigma \approx 4°$) into the same direction as is apparent from the p-orbital directions displayed by *Fig. 4*, *c*.

From a quantum-chemical-hybridization point of view, one would expect $sp^2\sigma$ hybridization plus a $p\pi$ orbital for the C-atoms in the anthracene rings with a single electron in each of the four L-shell AOs. Instead, the promolecule model presented here *presumes* that the 1s and 2s orbitals both doubly occupied. There are several reasons for this choice. First and foremost, promotion of a 2s electron to the 2p orbitals

would involve a strong electronic excitation by *ca*. 8 eV and, hence, not conform to the principle of forming independent atom promolecules from *oriented atomic ground-state ensembles*. Furthermore, this considerable energy difference not withstanding, the radial density distributions of 2s and 2p orbitals in momentum space are very similar and, therefore, difficult to distinguish by X-ray diffraction. Furthermore, in the molecules investigated so far, density-fitting in direct space with variable s/p-occupation has invariably yielded high s-populations near 2. These observations reveal significant differences between energy-based minimizations, which underlie all quantum-chemical interpretations, and density-based minimizations, which underlie all crystallographic analyses, including the present one.

In view of the just mentioned density similarities, the density of a doubly occupied 2s orbital is closely equivalent, in the present context, to that of a singly occupied 2s orbital plus 1/3 electron in each of the three p-orbitals. On the basis of standard quantum-chemical intuition, one would, therefore, expect the density analysis to yield an additional equal population of 2/3 electron for each of the three atomic p-orbitals. This is not the case, however: *Table 8* shows, as was already noted, that the carbon 2pπ AO's have occupancies that are much lower, whereas the 2pσ AO's have occupancies that are significantly higher, and *Fig. 4* clearly exhibits the flat disc-like shapes of the density ellipsoids of the π-bonded C-atoms. This is also found to be the case at atom C(15) with an orientation corresponding to hyperconjugation with the anthracene ring. These surprising results are not due to any error in the work on this molecule: Very similar population differences will be found for the other molecules to be discussed below. Nor is it a flaw of the present method of analysis: we have found analogous results for density analyses (in direct space) of quantum-mechanically calculated wave functions of individual molecules. We shall discuss the fundamental reasons for this remarkable feature of the density analyses of pπ-bonds in *Chapt. 5*.

4.1.4. *TBA Difference Densities* (*Fig. 5*). The total and the deformational difference density maps (TDD and DDD, respectively) of TBA are shown in *Fig. 5*, *a* and *b*. They were obtained by subtraction of spherical and oriented atom structure factors, respectively, from the experimentally determined structure factors and then *Fourier* transformation. Because of the nonplanarity of the molecule, the density is plotted on a roof-like surface formed by the two planes through the left and the right halves of the molecule. The maps exhibit the electron-density contribution *not* modeled by the oriented promolecule parameters.

The intramolecular interactions in the anthracene ring exhibit a significant amount of symmetry resulting in similar bond lengths. This *intra*molecular symmetry is well-reflected both by the AO *occupations* (similar q parameters) and by the deformational difference-density map (DDD in *Fig. 5*, *b*). The AO *directions,* on the other hand, and the TDD maps seem to be somewhat influenced by the asymmetric *inter*molecular interactions.

The bonding regions between the C-atoms exhibit a consistent DDD-contour level of 0.4 to 0.5 e/Å^3 and are well-centered on the C–C vectors. The bond density maxima in the TDD map vary somewhat more, between 0.5 to 0.7 e/Å^3. In addition, there is a little more density on the left-ring plane than on the right-ring plane, corresponding to the p-parameters on the left side being, on the average, 0.1 larger than those on the right side, which, however, is just the magnitude of $\sigma(q)$.

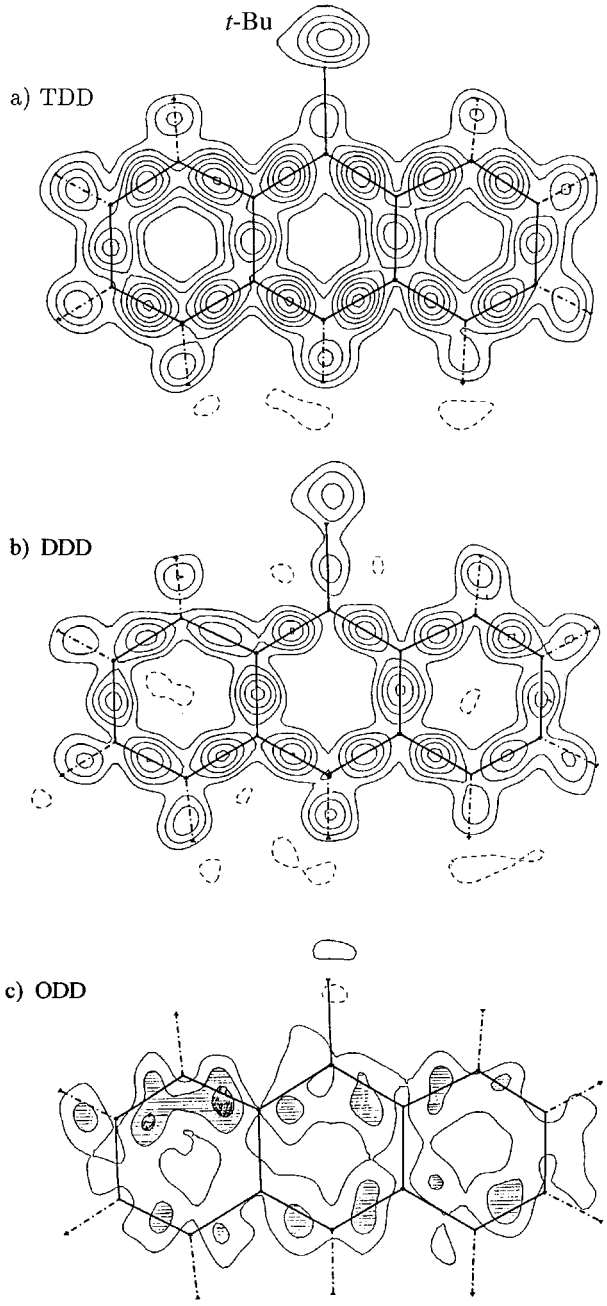

Fig. 5. *TDD Map* (*a*), *DDD map* (*b*), *and ODD map* (*c*), *on two roof-like planes through the left and right halves of TBA*. Contour lines described in legend of *Fig. 2*.

The different π to σ density transfer is also exhibited in the molecular plane of *Fig. 5,c*, which displays the ODD (= TDD − DDD). It reflects contacts of varying strengths between the molecule and its neighbors in the crystal.

4.2. ***Tetrafluoroterephthalonitrile (TFT).*** 4.2.1. *TFT Refinement.* A summary of the crystallographic information for tetrafluoroterephthalodinitrile (data from [67–69]) is given in *Table 6* and a drawing of the promolecule model is shown in *Fig. 6*. Previous studies have shown the X-ray data set to be a very good one, and comparisons with theoretical calculations are favorable [61][70]. Each of the atoms in TFT has a similar scattering power and there are no H-atoms.

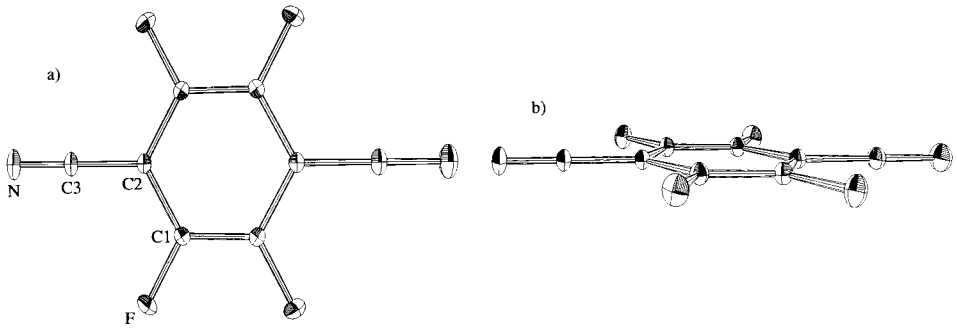

Fig. 6. *Top* (*a*) *and side* (*b*) *views of ellipsoid representation of tetrafluoroterephthalonitrile (TFT) representing atomic positions, and vibrational directions and amplitudes*

There are very few parameters in the promolecule model due to the high crystallographic symmetry (2/*m*) of the molecule. The ring exhibits rms deviation from planarity of only 0.004 Å. The atoms N, C(3) and C(2) lie on a mirror plane normal to the ring. The high site symmetry places severe constraints on the coordinates, thermal parameters, and valence parameters of the N, C(3), and C(2)-atoms. These constraints are handled as described in connection with *Eqn. 12* and by *Miller* [13].

The scale factor and the atomic positional and thermal parameters (37 in total) were refined against the 1133 HO data above 0.85 $Å^{-1}$ yielding results similar to those obtained by the authors of the original measurements. Following this initial refinement, the 19 valence-orbital parameters and one extinction parameter were simultaneously refined against the entire dataset.

4.2.2. *TFT Core Parameters* (*Fig. 6*). Due to the F and CN substitutions, the benzene ring no longer has D_{6h} symmetry. The C(1)–C(1′) bond lengths are slightly shorter (1.384 Å) than the C(1)–C(2) ones (1.395 Å), and C(2)–C(3) is significantly shorter (1.427 Å) than a typical single bond. Both have been interpreted as evidence of a slight quinoidic character [61][70].

4.2.3. *TFT Valence AO Parameters* (*Figs. 7 and 8,c*). The valence density of a N-atom is spherically symmetric in its $p^3\,{}^4S$ ground state. However, there exists a low-lying degenerate ^2D excited state in the p^3 ground-configuration manifold, which allows intra-atomic p-orbital electron transfer also at the N-atom for little energetic expense. Therefore, we use the $p^3\,{}^4S$ ground-state AOs, but allow for some $p\pi \rightarrow p\sigma$ electron transfer. The standard deviations of the refined occupancies are quite small, ranging

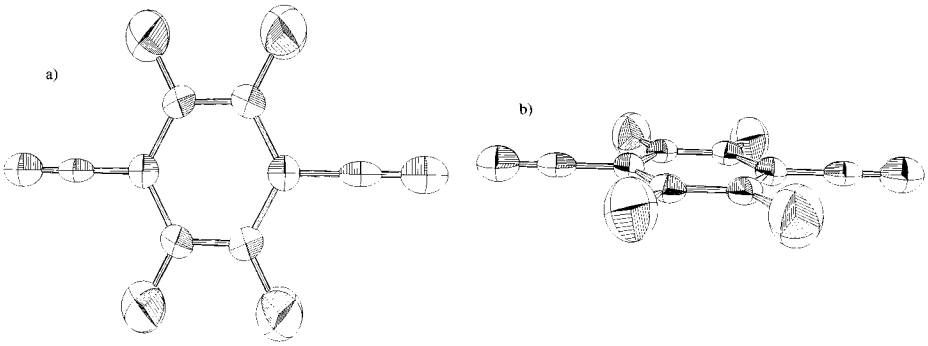

Fig. 7. *Top* (*a*) *and side* (*b*) *views of ellipsoid representation of atoms in TFT representing atomic positions, and valence-orbital directions and occupancies.*

Table 9. *Valence-Orbital Parameters for TFT* (see legend of *Table 8*). Standard deviations in brackets[a]).

Atom, q		π-AO	t or π'-AO	r-AO
C(1)	N_i	0.38(2)	0.98(2)	0.64(2)
$q=-0.43$	'r'	0.07	−0.15	0.99
or 0.47	't'	0.04	0.94	0.15
	'v'	0.99	−0.03	−0.07
C(2)		0.47(3)	0.74(3)	0.79(3)
$q=-0.29$		0.09	0.00	0.99
		0.00	1.00	0.00
		0.99	0.00	−0.09
C(3)		0.36(3)	0.36(3)	1.28(3)
$q=0.92$		0.00	0.00	1.00
		0.00	1.00	0.00
		1.00	0.00	0.00
N		0.77(2)	0.76(3)	1.47(3)
$q=0.69$		−0.01	0.00	1.00
		0.00	1.00	0.00
		1.00	0.00	0.01
F		1.75(1)	1.65(1)	1.60(1)
$q=0.12$		−0.23	0.22	0.95
or −0.10		−0.38	0.87	−0.30
		0.89	0.43	0.12

[a]) (n) means $\sigma=0.0$n.

from 0.01e to 0.03e (see the numbers in brackets listed in *Table 9*), confirming the high quality of this data set.

The valence-orbital-basis vectors used in *Table 9* are: 't' ≡ tangential-to, 'v' ≡ vertical-to, and 'r' ≡ radially-outward from the ring. The optimized valence-orbital arrangements that best fit the crystal density are shown in *Fig. 7*. The atoms N and C(3) have approximately prolate cylindrical symmetry, nearly parallel to the nitrile bond, which is consistent with our chemical intuition. As in TBA, the pπ-occupations of

these two atoms are much lower than their pσ-occupations. Their quadrupolarities are $q = N_\sigma - \bar{N}_\pi$ are 0.69 and 0.92 for N and C(3), respectively. The corresponding values obtained from quantum-chemical calculations and direct density-fitting on the isolated molecule are 0.70 and 0.73.

The valence-orbital arrangement for the C(2)-atom has oblate *cylindrical* symmetry with respect to an axis normal to the plane of the ring ($q = -0.29$, close to the quantum-mechanical value of 0.30 for the isolated molecule), which is consistent with the oblate ring atoms of TBA as discussed earlier, and of 1,2,3-triazine to be discussed later. The C(1) ring atom, however, has lost the axial symmetry, as shown by $N_{tangential} > N_{radial} > N_\pi$. That is, it is compressed by the electron-rich F-ligand in the radial direction. In such cases the q-parameters, especially their signs, are not well-defined (see *Table 9*).

The F-atom is quite close to being spherically symmetric, as is to be expected for a negatively charged F^-. Nonetheless, we have fixed the total p-occupations of the F-atoms, *i.e.*, neutral F to be 5. There are several reasons for this. First, our reference model is an atomic and not an ionic one. Second, the density distributions of even the most strongly ionic compounds such as those of the alkali halides are well-simulated by a superposition of neutral atoms [20][55][58]. Note also that, when an atom is nearly spherical (small q-parameter and nearly identical populations of the three p-AOs), then the AO-directions are not well-defined and are physically less significant.

A good theoretical correlation betwen pσ-population and bond order has been documented [15]. Accordingly, the populations found here (see also *Fig. 8*, *c*) indicate a stronger bond for C(1)–C(1′) than for C(1)–C(2) (average $\bar{N}_{\sigma(t)}$ bigger and average $\bar{N}_\pi$ smaller for C1–C1′), and some multiple bond character for C(2)–C(3) (large average $\bar{N}_{\sigma(r)}$ and small average $\bar{N}_\pi$). This is in agreement with the bond lengths.

4.2.4. *TFT Difference Densities* (*Fig. 8*). The total difference-density map with respect to spherically averaged atoms, shown in *Fig. 8*, *a*, exhibits a *large* build-up of charge along the bonds in the benzene ring and the nitrile bonds (being compensated by opposite TDD values in various other regions), and *small* (positive and, even, negative) contributions on the C(1)–F bond lines. Refining also the valence AO occupations and directions reduces the residuals and least-squares error of the independent atom model by as much as 50% (see *Table 6*). This means that the total information in the TDD as regards bonding has been split up in two parts of approximately equal magnitudes, one embodied in the numerical values of the valence AO orientations and occupations of the independent atoms in the crystal, the other being the DDD (and noise) shown in the map of *Fig. 8*, *b*. The overall effect of the valence AO orientations and occupations is exhibited by the ODD shown in *Fig. 8*, *c*.

The DDD map shows bond-charge accumulations of various magnitudes in *all* intramolecular bonds. Since the present maps are dynamic ones, the features are thermally smeared and are less pronounced than in theoretical static maps. Indeed, density-fitting in direct space for the quantum-mechanical wave function of the isolated $C_8F_4N_2$ molecule yields a DDD map with a maximum of 0.2e/Å^3 in the C–F bonds. For the C–F bonds of some other molecules, too, *negative* values have been found on the TDD maps [68][71], whereas DDD maps always exhibit positive values [15].

The very low DDD maxima in the C(2)–C(3) and C(2)–N nitrile bonds deserve a comment. While, in general, density deformations and orbital occupations can be unambiguously distinguished, that is not the case for digonal, linear coordination. This

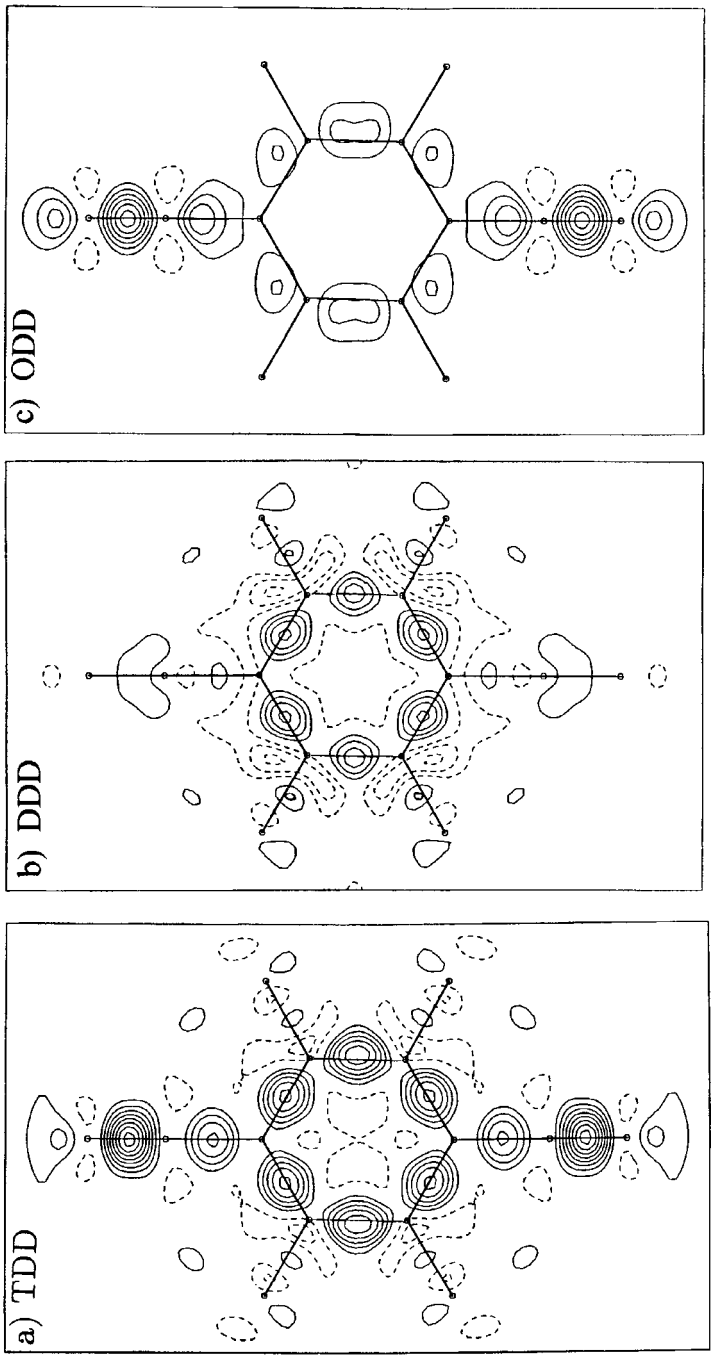

Fig. 8. *TDD Map* (*a*), *DDD map* (*b*), and *ODD map* (*c*) *of TFT*. Contour lines described in legend of *Fig. 2*.

is so because in the least-squares procedure, density accumulations corresponding to covalence or lone pairs *in two opposite directions* can be largely simulated by an increased pσ-occupation, with the consequence that the DDD is small. Hence, digonal multiple bonds and lone pairs result in low deformation difference densities [15]. In these cases, the covalent bond strength correlates with the π to σ occupation transfer rather than with the DDD bond charge, as can be seen in *Fig. 8*, *b* or *c*.

4.3. *1,2,3-triazine (TA).* 4.3.1. *TA Refinement.* A summary of the crystallographic information for 1,2,3-triazine [72] is given in *Table 6*. Drawings of the positions and vibrations of the promolecule reference were shown in *Fig. 1*, *a*.

As a compromise, a STOL cutoff of 0.6 $Å^{-1}$ was used. This cutoff left 1137 reflections for the determination of the 55 core-type parameters. The statistical results of the refinement of the core-type parameters against the HO data and the simultaneous refinement of the 42 valence-type parameters against the entire data set are given in *Table 6*, the resultant parameters are given in *Table 10*.

4.3.2. *TA Core Parameters* (*Fig. 1*, *a*). Despite the asymmetric crystal surroundings, the molecular rings are planar and left-right symmetric within 0.001 Å ($\sigma = 0.001$ to

Table 10. *Valence-Orbital Parameters for TA* (see legend of *Table 8*). Standard deviations in brackets[a]).

Atom		π-AO	*t*-AO	*r*-AO
N(1)	N_i	0.58(4)	0.93(4)	1.49(3)
	'*r*'	0.20	− 0.27	0.94
	'*t*'	− 0.72	0.61	0.33
	'*v*'	0.66	0.74	0.08
N(2)		− 0.76(3)	1.02(4)	1.22(3)
		0.24	− 0.16	0.96
		0.22	0.97	0.10
		0.94	− 0.19	− 0.27
N(3)		0.61(3)	0.92(4)	1.47(3)
		0.33	0.47	0.82
		0.42	0.71	− 0.57
		0.85	− 0.53	− 0.04
C(1)		0.38(4)	0.62(4)	1.00(4)
		0.03	0.59	0.81
		0.23	0.78	− 0.58
		0.97	− 0.20	0.11
C(2)		0.38(4)	1.03(4)	0.59(4)
		0.77	0.05	0.63
		0.03	0.99	− 0.12
		0.63	− 0.11	− 0.76
C(3)		0.21(4)	0.67(4)	1.17(4)
		0.15	0.88	− 0.45
		0.02	0.45	0.89
		0.99	− 0.14	0.05

[a]) (n) means $\sigma = 0.0$n.

0.002 Å), while the H-atoms are asymmetrically shifted. Bond length/bond order relations yield the following bond orders: 1.7(1) for C–C, 1.5(7) for N–N, and 1.5(3) for C–N.

4.3.3. *TA Valence AO Parameters* (*Fig. 1,b*). The atoms in triazine have rather asymmetric densities (*Table 10*) that cannot be represented by a single q-parameter. The average occupancies of the N-atoms are N$p\pi \sim 0.65$e, N$pt \sim 0.95$e, and N$pr \sim 1.4$e ($\sigma(N_i) = 0.03$ to 0.04e). In close correspondence, fitting of the quantum-mechanically isolated molecule density yields the values 0.71e, 0.94e, and 1.35e. The π-occupancies are again relatively low, but higher than those of the π-bonded C-atoms corresponding to the higher electron numbers of the N-atoms. The highest occupancies are radially outward in the directions of the N lone pairs. However, owing to N···HC intermolecular interactions in the crystal, they are somewhat bent away from the radial directions.

The average carbon π-occupation is C$p\pi \sim 0.3$e, in agreement with the conjugated carbons in the other molecules. Similarly, fitting of the theoretical density of the single molecule yields 0.29e. The occupancy of the carbon AOs nearest to the C–C bonds (C(1)*pr*, C(2)*pt*, C(3)*pr*; see *Table 10* and *Fig. 1,b*) is ~ 1.05e. Density fitting of the calculated isolated-molecule wave functions yields the theoretical value 0.90e. The magnitude of the density increase in the bonds due to valence-shell orientation (*Fig. 2,c*) varies in the order C–C > N–N > C–N. This corresponds to the bond orders deduced from the core parameters.

As is the case for the layer structured TBA, all atoms in TA are also tilted in the same direction, in fact about 25° (*Fig. 1,b*). The molecular-packing effects, although much weaker than the chemical bonds, are still easily detectable. They have an interesting influence on the direction of the atomic orbitals, which will be discussed in more detail elsewhere.

4.3.4. *TA Difference Densities* (*Fig. 2*). The free TA molecule has C_{2v} symmetry with the C_2-axis passing through the atoms N(2), C(2), H(2). This is not reflected at all in the TDD map. Indeed, due to molecular packing and intermolecular interactions, the C_2 axis of the free molecule is not maintained in the crystal. Nonetheless, equivalent bonds have still nearly identical lengths implying that, in spite of the *inter*molecular interactions in the crystal, the *intra*molecular bonding situation is nearly unchanged. This inference is indeed confirmed by the approximate symmetry of the DDD map.

5. Density Fitting and Quantum-Mechanical Populations: Inferences from the π-Bonded p-Occupancies. – A startling result found in the preceding sections was that all carbon p-AO's involved in π-bonding are assigned much lower *occupancies* in the oriented-atom-density model than one would anticipate from *population* analyses of quantum-mechanical wave functions. We encountered this apparent discrepancy first for the occupancies deduced from experimental X-ray data on crystals [13], but subsequently obtained entirely analogous results for promolecule densites determined, as discussed above, by fitting to theoretically calculated *ab initio* densities of corresponding isolated molecules in direct space [15][25][28]. We shall now show that this occupation/population difference reveals a basic difference in character between those orbital expansions that are obtained by fitting a molecular *electronic density* through a superposition of atomic-orbital densities, and those orbital

expansions that are determined by the first-order *density matrix* of the electronic wave function.

The orbital populations deduced from an electronic wave function provide information regarding the electron distribution that is derived from the expansion of the first-order density *matrix* $D(r_1, r_2)$ in terms of these orbitals. Relevant in the present context are expansions in terms of *optimally adapted, fully or partially occupied atomic orbital* sets (say, by expansion in terms of extended bases). For most molecules, it is possible to find good approximations to the exact density matrix that can be expressed in this manner (*e.g.*, by full-valence-space MCSCF calculations). Such expansions can be written in the form

$$D(r_1, r_2) = \Sigma_{ij}\chi_i(r_1)\chi_j(r_2)p_{ij} = D^0 + \Delta D, \tag{18}$$

$$D^0 = \Sigma_i\chi_i(r_1)\chi_i(r_2)q_i,\ q_i = \Sigma_j p_{ij}S_{ij},\ S_{ij} = \langle\chi_i \,|\, \chi_j\rangle, \tag{19}$$

$$\Delta D = \Sigma_{ij}[\chi_i\chi_j - S_{ij}(\chi_i\chi_j + \chi_j\chi_j)/2]p_{\mathrm{ij}} \tag{20}$$

where the elements p_{ij} form the so-called charge-bond-order matrix. The terms D^0 and ΔD are the quasiclassical and the interference parts, respectively, of the density matrix [23]. Since ΔD vanishes upon integration over all space, D^0 contains the entire electron population, and *the weight factors* q_i *in the quasi-classical part* D^0 *are the* Mulliken *populations of the optimal atomic minimal orbital set*. (Similar statements also hold for more advanced population definitions.) We note that two basic properties of the density matrix expansion are accounted for, namely *i*) that the density matrix is derived from an antisymmetric wavefunction, *i.e.*, that it satisfies the demands of the *Pauli* principle, and *ii*) that parts of the populations arise from off-diagonal terms of D, *i.e.*, from products of atomic orbitals on different atoms with nonvanishing overlap integrals.

Much less information is available, on the other hand, if only the density (*i.e.*, $r_1 = r_2$ in *Eqn. 18*) is known, be it in position space, in momentum space, or in both. This information is, in fact, insufficient for the reconstruction of the total density matrix (see, *e.g.*, [7][8]). *The deduction of atomic orbitals and their occupancies from densities alone requires*, *therefore*, *additional constraints introducing further assumptions. In all crystallographic promolecule models*, *for instance*, *only atomic one-center terms are admitted* (with variable occupancies, and, possibly, radial scaling and angular deformations) because strong indeterminacies are encountered when one attempts to include two-center overlap terms as well [4][7]. As a result, serious problems can arise with respect to the *Pauli* principle and the interatomic-overlap contributions, as we shall now see by examining a specific example.

Consider the ethylenic prototype model of two equivalent C-atoms, *a* and *b*, connected by a σ- as well as by a π-bond. All other bonds and electrons are ignored. An approximate molecular-density matrix D and density ρ are given by

$$D(r_1, r_2) = D_\sigma + D_\pi,\ D_\sigma = 2\sigma(r_1)\sigma(r_2),\ D_\pi = 2\pi(r_1)\pi(r_2), \tag{21}$$

$$\rho_{\mathrm{mol}}(r) = \rho_\sigma + \rho_\pi,\ \rho_\sigma = 2[\sigma(r)]^2,\ \rho_\pi = 2[\pi(r)]^2, \tag{22}$$

with the molecular orbitals

$$\sigma = (\sigma_a + \sigma_b)/\sqrt{2(1+S_\sigma)},\ S_\sigma = \langle \sigma_a \,|\, \sigma_b \rangle,$$

$$\pi = (\pi_a + \pi_b)/\sqrt{2(1+S_\pi)},\ S_\pi = \langle \pi_a \,|\, \pi_b \rangle, \tag{23}$$

where σ_a, σ_b are σ-AO's on atoms *a* and *b* respectively, parallel to the bond axis and pointing towards each other, while π_a, π_b are π-AO's perpendicular to the a–b bond.

In analogy to *Eqn. 18*, the molecular-density can then be expressed as the sum of a quasiclassical part σ^0 and an interference part $\Delta\rho$:

$$\rho_{mol} = \rho^0 + \Delta\rho,\ \rho^0 = \rho_\sigma^0 + \rho_\pi^0,\ \Delta\rho = \Delta\rho_\sigma + \Delta\rho_\pi, \tag{24}$$

$$\rho_\sigma^0 = \sigma_a^2 + \sigma_b^2,\ \Delta\rho_\sigma = [2\sigma_a\sigma_b - S_\sigma(\sigma_a^2 + \sigma_b^2)]/(1+S_\sigma),$$

$$\rho_\pi^0 = \pi_a^2 + \pi_b^2,\ \Delta\rho_\pi = [2\pi_a\pi_b - S_\pi(\pi_a^2 + \pi_b^2)]/(1+S_\pi). \tag{25}$$

Separate integrations of ρ_σ^0 as well as ρ_π^0 yield two electrons in each case. The coefficients of the squares of the AOs in ρ_σ^0 and ρ_π^0 (*Eqn. 25*) are the *Mulliken* populations. They are manifestly *unity for every one of the four atomic orbitals* and, at the SCF level, this is independent of the quality of the orbitals.

Assume now that only the density ρ_{mol} is known and consider the approximation obtained by fitting to it a promolecule density ρ_{pm} *in terms of atomic-orbital densities with the same atomic orbitals* σ_a, σ_b, π_a, π_b. The $D_{\infty h}$ symmetry forces σ_a^2 and σ_b^2 to have equal occupancies and the same holds for π_a^2 and π_b^2. Hence, in contrast to *Eqn. 24*, the density of the fitted promolecule will have the form

$$\rho_{pm} = q_\sigma\rho_\sigma^0 + q_\pi\rho_\pi^0,\ q_\sigma + q_\pi = 2, \tag{26}$$

where ρ_σ^0, ρ_π^0 are the quasiclassical density parts defined in *Eqn. 25*, and q_σ, q_π do not have to be 1. It is apparent that q_σ and q_π are also the *occupancies* of the corresponding individual *atomic-orbital densities* in the model. Satisfaction of the *Pauli* principle separately on each atom requires therefore that q_σ and q_π both lie between 0 and 2, and we can write

$$q_\sigma = 1 + \cos\gamma,\ q_\pi = 1 - \cos\gamma, \tag{27}$$

so that the promolecule density can be expressed as

$$\rho_{pm} = \rho^0 + \rho'\cos\gamma,\ \rho' = \rho_\sigma^0 - \rho_\pi^0, \tag{28}$$

with ρ^0 being the quasiclassical density of *Eqn. 24*.

The difference between the molecular-density ρ_{mol} in *Eqn. 24* and the promolecule density of *Eqn. 28* depends, therefore, on the one parameter γ as follows

$$\rho_{mol} - \rho_{pm} = \Delta\rho - \rho'\cos\gamma, \tag{29}$$

and the least-mean-squares fit of ρ_{pm} to ρ_{mol} is readily seen to be accomplished by the value of γ satisfying

$$\cos\gamma = Q \text{ if } |Q| < 1, \cos\gamma = Q/|Q| \text{ if } |Q| > 1, \tag{30a}$$

$$Q = \langle \Delta\rho \,|\, \rho' \rangle / \langle \rho' \,|\, \rho' \rangle. \tag{30b}$$

The promolecule occupancies will therefore agree with the *Mulliken* populations (*i.e.*, $q_\sigma = q_\pi = 1$) only when $\cos\gamma = \langle \Delta\rho \,|\, \rho' \rangle = 0$, *i.e.*, if

$$\langle \rho_{mol} - \rho_\sigma^0 \,|\, \rho_\sigma^0 \rangle = \langle \rho_{mol} - \rho_\pi^0 \,|\, \rho_\pi^0 \rangle \tag{31}$$

which is manifestly not the case in general. In fact, model calculations with typical atomic orbitals at reasonable interatomic distances always yield positive values for $\cos\gamma$. According to *Eqn. 27*, this result implies σ occupancies larger than unity and π occupancies smaller than unity, in agreement with what was found in our investigation of actual molecules and crystals.

The origin of this σ-occupancy excess and the corresponding π-occupancy deficiency, as compared with the *Mulliken* populations, becomes apparent by considering *Eqns. 24*, *25*, and *28*, *29*. Whereas the density from the wave function contains two-center-overlap interference contributions ($\Delta\rho$ in *Eqns. 24* and *25*), the promolecular density contains only pure atomic terms. LMSQ Minimization of the difference (*Eqn. 29*)] implies, therefore, that the interference density contribution $\Delta\rho$ to ρ_{mol} will be mimicked by ρ', defined in *Eqn. 28*, *i.e.*, by a readjustment of the quasiclassical density contributions ρ_σ^0 and ρ_π^0 to ρ_{pm}. Since ρ_σ^0 contains a greater charge density in the bond center than ρ_π^0, it is better suited to substitute for the interference density, which embodies a charge accumulation around the bond center. The ρ_σ^0 occupancy is, therefore, enhanced at the expense of the ρ_π^0 occupancy. (Similar simulations are also found for higher quality density fittings such as in multipole models.)

The occupancy shift described is *possible* since, in the independent-atoms promolecule, the *Pauli* principle is enforced *only within each atom*. In the actual SCF wave function on the other hand, the σ populations as well as the π populations *both* must be equal to unity because of the validity of the *Pauli* principle *in the molecule* (see *Eqns. 21* and *22*). There is no analogous restriction in the promolecule model. (The main thrust of these inferences also remain valid for post-SCF wave functions even though the constraints on the populations are less rigid there because of the possibility of some $\sigma^2 \rightarrow \pi^{*2}$ substitutions.)

In addition to the foregoing considerations, a further factor must be taken into account with respect to the promolecule densities used in our analysis, namely, that the promolecule-density fitting is done, by definition, in terms of *free-atom* SCF orbitals, whereas the atomic orbitals required for the optimal representation of the molecular-density matrix may be severely deformed with respect to the free-atom orbitals, notably by radial scale changes and by angular polarizations. Such atomic-orbital deformations do not alter, the population distribution between the p- and the s-orbital space determined by the *actual* SCF density matrix. But, use of the free-atom SCF orbitals for fitting the promolecule density to such an actual density entails an even greater

preference of the σ contributions over the π contributions by virtue of the aforementioned lack of restrictions. (Additional changes occur at post-SCF levels or using experimental densities.) These further enhancements of the trend explained in the preceding paragraphs can be quite large, as is documented in a detailed examination of a variety of theoretically calculated double-bond densities [25][28].

Thus, intrinsic differences exist between atomic-orbital *occupancies* determined by promolecule density fittings and atomic-orbital *populations* determined by density-matrix expansions. They arise from the absence, in the promolecule model, of the interatomic-overlap terms and the interatomic electron-sharing restrictions related to the *Pauli* principle. They are furthermore exacerbated by molecular deformations of the atomic-orbital bases.

6. Discussion. – **6.1.** ***Procrystal Specifications.*** An algorithm has been described for the least-squares determination of the parameters of a promolecule constructed from *positioned and oriented* independent atoms, and its usage has been illustrated. The promolecule's standard core-type parameters (non-H-coordinates, vibrations, and site occupancies) are determined for the atoms with core shells (which are largely unaffected by chemical-bonding effects) using the high-order data. In addition, our promolecule includes valence-type parameters (the usual H parameters as well as the valence-orbital occupancies, and the shapes and orientations of all heavier atoms) and they are determined on the basis of the entire data set in the least-squares refinement. We note that the valence density comprises extended as well as sharply localized features in the bonds and lone pairs. No significant interactions between the core parameters from the high-order data, and the valence-orbital parameters have been found so far in simultaneous refinements. The oriented-atom promolecule offers additional insight into the nature of chemical bonding.

Atomic coordinates and vibrational parameters are the major indicators for recognizing interatomic interactions, characterizing both intramolecular bonds and intermolecular interactions [73]. We mention, for instance, the bond length-bond order relation. The electrostatic quasiclassical interaction of independent atoms at quantum-mechanical equilibrium separations contributes a major portion of the equilibrium bond energy [16][17][36].

In the present model of atoms in molecules and crystals, the second largest effect on the density of systems with open valence-shell atoms is due to the establishment of specific *ground-state* orientations and occupations in the valence shells of atoms with degenerate or quasi-degenerate ground states. The AO occupations are strongly influenced by the *Pauli* exclusion effect of doubly occupied AOs. This ground-state orientation of the independent atoms can change the quasi-classical electrostatic interaction energy by amounts of up to several eV per bond [17]. The atomic valence-orbital occupancies correlate well with bond orders and bond polarities [15].

The third piece of information of bonding is the remaining difference density (called here deformation difference density, DDD). It comprises those quantum-mechanical interference effects, charge transfers, and genuine atomic deformations (energy-costly atomic promotions paying out slightly more when the atoms bind), which cannot be simulated by appropriate orbital occupancies in the independent atom ground states.

There are many indications that it is intrinsically difficult to relate density differences in detail to energy differences. We note, for instance, the difficulties of finding density functionals that reproduce kinetic energies to an accuracy commensurate with molecular binding energies, or the practical impossibility of recovering quantum-mechanical wave functions from their densities without solving the *Schrödinger* equation. Relevant for the crystallographic context is that, so far, unambiguous density fittings are practically restricted to the use of superpositions of atomic densities. We have discussed in *Chapt. 5* that this limitation entails intrinsic differences in the interpretation of the resulting occupations as compared to populations deduced from quantum-mechanical wave functions.

Given this limitation, the described extraction of oriented ground-state densities (satisfying specific restrictions including the intra-atomic *Pauli* principle) by means of an optimal local-density adaptation seems a sound approach to the identification of meaningful intrinsic atomic building blocks in the promolecule/procrystal model. We have demonstrated its feasibility and performance by applying it to an interesting cross-section of systems. 9-(*tert*-butyl)anthracene, tetrafluoroterephthalonitrile, and 1,2,3-triazine. 9-(*tert*-butyl)anthracene (TBA) has low site symmetry but a very large redundancy of chemically similar bonding situations. Tetrafluoroterephthalonitrile (TFT), on the other hand, has high crystallographic symmetry and a variety of unique bonding situations. 1,2,3-triazine (TA), finally, has some redundancy and its low number of parameters permitted us to carry out a large number of tests when developing the method [13].

The investigations have shown that the densities of this oriented independent atoms model, as well as the resulting DDDs, exhibit consistent behavior patterns under analogous binding and coordination situations, and are amenable to consistent interpretations (even though their occupancies have somewhat different meanings than the populations derived directly from wave functions).

It is particularly gratifying and significant that a close agreement is found between the quantitative inferences drawn from fitting oriented-atom model densities of *isolated molecules to the densities of the calculated quantum-mechanical wave functions* and the quantitative conclusions reached from fitting the *Fourier* transforms of oriented-procrystal model densities to the *experimental X-ray diffraction data of the molecular crystals* formed from the same molecules. This parallelism is extremely useful because, through theoretical calculations on isolated molecules, it is possible to establish explicit relationships between the features of oriented promolecules as defined here and the population and bonding properties of quantum-mechanical wave functions in as much detail as is necessary or desirable. These isolated-molecule results can then serve to gauge the interpretation of oriented-atom models for procrystals derived from experimental densities.

6.2. ***Results for the Reference Model***. The new reference model exhibits information about chemical interactions between atoms in crystals that exceeds what is provided by bond lengths and angles derived from the core positional parameters alone. The new information is furnished by the directional parameters and the occupancies of the valence AOs. The asphericity of this reference model can also be exhibited by the orientational difference density (ODD), *i.e.*, the difference between the density of the

superposition of the optimally oriented and the spherically averaged atoms. The following trends were found: *1*) Short and strong bonds result in highly populated pσ-AOs with high occupations parallel to the bond, or tangential to two adjacent bonds. *2*) The π-bonds are generally characterized by pπ-AO occupations that are rather lower than corresponding populations derived from electronic wave functions. This general result is corroborated by density fittings of purely theoretically calculated wave functions of isolated molecules [15], and its reasons and implications have been discussed in *Chapt. 5*. *3*) Lone pairs also result in highly populated p-AOs oriented in the 'lone-pair direction'. *4*) Electron attracting, electron-rich atoms that are thought of as carrying a negative partial charge (such as F in TFT) are nearly spherical. They reduce the pσ-population of the adjacent atom. *5*) While the AO *occupancies* are essentially determined by the strong intramolecular bonds, the AO *orientations* are also influenced by the weaker intermolecular effects in molecular crystals.

For the interpretation of the orbital occupancies, it is furthermore relevant to keep in mind that p-orbitals are objects extending on two opposite sides of the atomic cores, while chemical building blocks such as bonds or lone pairs in general are thought to extend only to one side of the core, with various angles between them. Consequently, all bonds and lone pairs of one atom *together* determine the three p-occupancies in a coupled manner under the constraint of atomic charge conservation. In the special case where two such chemical building blocks are linearly coordinated, forming an angle of 180°, the corresponding pσ-AO acquires an especially high population.

From the foregoing observations, it is apparent that the role played by the atomic orbitals in the present context is somewhat different from that played in the context of quantum-chemical population analyses. The implication is that the oriented atomic orbitals and their occupations, as obtained from density fittings, cannot be directly identified with any natural atomic orbitals intrinsic to molecular electronic wave functions. This is because, in the context of X-ray-analysis work, all effective density fittings are based on the superposition of atomic densities, and, in such an approach, atomic orbitals are used somewhat differently than in molecular wave functions. Most consequential are the following two differences: *i*) densities of wave functions contain overlap and interference terms between different atoms whereas crystallographic density-fitting expressions do not and have to approximate them through superpositions of AO densities; *ii*) densities of wave functions embody certain restrictions placed on the sharing of electrons between different atoms as a result of the validity of the *Pauli* principle for the molecular wave functions, whereas the density-fitting expressions embody only the intra-atomic *Pauli* principle. However, although these differences entail modifications in the conceptual interpretations, such interpretations can nonetheless be developed in a consistent manner, as has been elaborated above, in particular with the help of theoretical calculations on isolated molecules.

6.3. ***Results for the Deformation Difference Density.*** The information remaining after subtracting the reference model density from the actual electron density is displayed by the deformation difference density (DDD), *i.e.*, the density difference between the crystal and the positioned and oriented independent atoms. In these maps the following trends were observed: *1*) *All* covalent bonds exhibit bond density accumulations in the DDD maps. Since the refined AO populations already account for

the atomic *Pauli* exclusion effects, even bonds to electron-rich atoms like F, which exhibit zero or negative bond charges in the traditional TDD maps, show at least some density accumulation in the DDD map. *2*) Strong or multiple bonds do *not* show bigger, but normal (*ca*. 0.4e/Å^3 for 2nd-row atoms, as C or N) or even smaller DDD values. This surprising result, which is also found in theoretical calculations on isolated molecules [20], is related to the fact that, as discussed above, these bonds have a high pσ-population of the model density, especially if there are bonds or lone pairs on the back side of the atom (≡N| in TFT, compare also –$\overline{\text{F}}$|). **If, now, such a strongly populated p-AO is subtracted from the molecular bond density, then only a low DDD value survives in the bond (C≡N**, C–F, and C_{ring}–CN of TFT, bonds of TA). *3*) DDD Accumulations behind the atoms (coupled with charge depletion on the opposite side of the core) indicate lone pairs. These typically *dipolar* features on DDD maps are, however, not as complex as the corresponding lone-pair features on TDD maps, which most often have *multipolar* character, of various signs that strongly depend on the chosen valence-AO populations (spherical or prepared). Again, it is to be noted that bonds, especially multiple bonds, opposite to a lone pair result in a large p-AO population which may leave only very little lone-pair density in the DDD (N and F in the TFT molecule). The influence of the C(3)≡N triple bond on the C(3)-pσ population similarly results in a low DDD value on the C(1)–C(2) single bond in TFT. *4*) Intermolecular interactions, which do not modify intramolecular bonds significantly, have only a small influence on the *intramolecular* DDD.

We gratefully acknowledge the authors of the papers by *Angermund*, *Claus*, *Goddard* and *Krüger* [65]; *Dunitz*, *Schweizer*, and *Seiler* [67]; and *Neunhöffer et al*. [72], especially *K. Angermund*, *J. D. Dunitz*, *R. Goddard*, *C. Krüger*, and *F. Seiler*, for sharing their high accuracy X-ray datasets. The authors are grateful to *D. Feil*, *B. Engelen*, *N. K. Hansen*, *T. Koritsanszky*, and *U. Bartsch* for constructive comments. This work was supported in part by *Ames Laboratory*, which is operated for the *U. S. Department of Energy* by Iowa State University under contract No. W-7405-ENG-82, funded by the *Division of Chemical Sciences* and the *Division of Materials Sciences*, *Office of Basic Energy Sciences*. The work was also supported by the *Deutsche Forschungsgemeinschaft* (grant No. Schw 161-30), by the *Fonds der Chemischen Industrie* (grant No. 160273), and by the *NATO* Grant No. 298/83.

REFERENCES

[1] A. J. Rocke, 'Chemical Atomism', Ohio State University Press, Columbus, 1984.
[2] J. Lima de Faria, 'Historical Atlas of Crystallography', Kluwer, Dordrecht, 1990.
[3] V. G. Tsirelson and R. P. Ozerov, 'Electron Density and Bonding in Crystals', Institute of Physics, Bristol, 1996.
[4] P. Coppens, 'X-Ray Charge Densities and Chemical Bonding', Oxford University Press, 1997.
[5] J. E. Harriman, *Z. Naturforsch., A* **1993**, *48*, 203.
[6] H. Schmider, V. H. Smith, W. Weyrich, *Trans. Amer. Cryst.* **1990**, *26*, 125; H. Schmider, V. H. Smith, W. Weyrich, *Z. Naturforsch., A* **1993**, *48*, 211, 221.
[7] W. H. E. Schwarz, B. Müller, *Chem. Phys. Lett*. **1990**, *166*, 621.
[8] W. H. E. Schwarz, A. Langenbach, L. Birlenbach, *Theor. Chim. Acta* **1994**, *88*, 437.
[9] L. Massa, L. Huang, J. Karle, *Int. J. Quantum Chem*. **1995**, *S29*, 375; L. Massa, L. Huang, J. Karle, *Int. J. Quantum Chem.* **1999**, *73*, 439.
[10] W. L. Clinton, A. J. Galli, L. J. Massa, *Phys. Rev*. **1969**, *177*, 7; W. L. Clinton, A. J. Galli, L. J. Massa, *Phys. Rev. Lett*. **1972**, *73*, 1363.
[11] D. Jayatilaka, *Phys. Rev. Lett*. **1998**, *80*, 798.
[12] D. Jayatilaka, D. J. Grimwood, *Acta Crystallogr.*, *Sect. A* **2001**, *57*, 76, 87.
[13] L. L. Miller, Ph.D. Thesis, Ames (IA, USA), Iowa State University; and USDOE Report No. IS-T-1341, 1988.

[14] J. E. Niu, 'Elektronenverteilungen in Atomen, Molekülen und Kristallen', Ph.D. Thesis, University Siegen, Shaker Press, Aachen, 1994.
[15] W. H. E. Schwarz, H. L. Lin, S. Irle, J. E. Niu, *J. Mol. Struct. (Theochem.)* **1992**, *255*, 435.
[16] M. A. Spackman, E. N. Maslen, *J. Phys. Chem*. **1986**, *90*, 2020.
[17] S. G. Wang, W. H. E. Schwarz, H. L. Lin, *Chem. Phys. Lett.* **1991**, *180*, 509.
[18] R. F. W. Bader, in 'The Force Concept in Chemistry', Ed. B. M. Deb, Van Nostrand Reinhold, New York, 1981, p. 39.
[19] H. Bruning, Internal Report, University Siegen, Germany, 1993.
[20] S. Irle, H. L. Lin, J. E. Niu, W. H. E. Schwarz, *Ber. Bunsen-Ges. Phys. Chem*. **1992**, *96*, 1545.
[21] L. Mensching, L. L. Miller, P. Valtazanos, K. Ruedenberg, W. H. E. Schwarz, W. von Niessen, R. Jacobson, *Angew. Chem.* **1989**, *101*, 605; *Angew. Chem.*, *Int. Ed*. **1989**, *28*, 597.
[22] L. Mensching, W. von Niessen, P. Valtazanos, K. Ruedenberg, W. H. E. Schwarz, *J. Am. Chem. Soc*. **1989**, *111*, 6933.
[23] K. Ruedenberg, *Rev. Mod. Phys.* **1962**, *34*, 326.
[24] H. Möller, J. E. Niu, H. D. Lutz, W. H. E. Schwarz, *J. Mol. Struct*. **1997**, *436/7*, 233.
[25] J. E. Niu, W. H. E. Schwarz, K. Ruedenberg, *J. Mol. Struct. (Theochem)* **1997**, *389*, 117.
[26] J. E. Niu, W. H. E. Schwarz, *Chem. Phys. Lett*. **1996**, *249*, 218.
[27] S. Irle, M. T. Krygowski, J. E. Niu, W. H. E. Schwarz, *J. Org. Chem*. **1995**, *60*, 6744.
[28] J. E. Niu, W. H. E. Schwarz, *J. East China Normal Univ. (Nat. Sci*) **1993**, *2*, 48.
[29] S. Irle, Masters Thesis, University Siegen, 1992.
[30] W. H. E. Schwarz, L. Mensching, K. Ruedenberg, R. Jacobson, L. L. Miller, *Portgal. Phys.* **1988**, *19*, 185.
[31] W. H. E. Schwarz, L. Mensching, P. Valtazanos, W. von Niessen, *Int. J. Quantum Chem.* **1986**, *30*, 439.
[32] W. H. E. Schwarz, P. Valtazanos, K. Ruedenberg, *Theor. Chim. Acta* **1985**, *68*, 471.
[33] K. Ruedenberg, W. H. E. Schwarz, *J. Chem. Phys.* **1990**, *92*, 4956.
[34] W. H. E. Schwarz, K. Ruedenberg, L. Mensching, *J. Am. Chem. Soc*. **1989**, *111*, 6926.
[35] J. Meister, Masters Thesis, University Siegen, 1997.
[36] F. L. Hirshfeld, S. Rzotkiewics, *Mol. Phys.* **1974**, *27*, 1319.
[37] W. H. E. Schwarz, *Portgal. Phys.* **1988**, *19*, 429.
[38] K. Angermund, Ph.D. Thesis, Universität Wuppertal, Wuppertal, Germany, 1986.
[39] P. J. Becker, P. Coppens, *Acta Crystallogr.*, *Sect. A* **1974**, *30*, 129, 148.
[40] Y. Le Page, E. J. Gabe, *J. Appl. Crystallogr*. **1978**, *11*, 254.
[41] G. H. Stout, L. H. Jensen, 'X-Ray Structure Determination', John Wiley & Sons, New York, 1968.
[42] W. H. Zachariasen, *Acta Crystallogr*. **1963**, *16*, 1139.
[43] D. E. Sands, 'Vectors and Tensors in Crystallography', Addison-Wesley, London, 1982.
[44] M. F. C. Ladd, R. A. Palmer, 'Structure Determination by X-Ray Crystallography', Plenum, New York, 1978.
[45] D. T. Cromer, J. T. Waber, in 'International Tables for X-Ray Crystallography', Eds. J. A. Ibers & W. C. Hamilton, Kynoch Press, Birmingham, Vol. IV, p. 71, 1974.
[46] G. Arfken, 'Mathematical Methods for Physicists', Academic Press, New York, 1985, p. 573.
[47] R. C. Raffenetti, *J. Chem. Phys.* **1973**, *59*, 5936.
[48] R. C. Raffenetti, K. Ruedenberg, 'Even-Tempered Representations of Atomic Self-consistent Field Wavefunctions', USAEC Report No. IS-3195, 1973.
[49] M. Weissbluth, 'Atoms and Molecules', Academic Press, New York, 1978.
[50] M. Rotenberg, R. Bivins, N. Metropolis, K. Wooten, 'The 3j and 6j Symbols', MIT Press, Cambridge, 1959.
[51] S. R. Hall, T. Ashida, 'Methods and Applications in Crystallographic Computing', Clarendon, Oxford, 1984.
[52] D. Sayre, 'Computational Crystallography', Clarendon, Oxford, 1982.
[53] G. M. Sheldrick, C. Krüger, R. Goddard, 'Crystallographic Computing 3', Clarendon, Oxford, 1985.
[54] W. J. A. M. Peterse, J. H. Palm, *Acta Crystallogr*. **1966**, *20*, 147.
[55] B. Hess, H. L. Lin, J. E. Niu, W. H. E. Schwarz, *Z. Naturforsch*. **1993**, *48a*, 180.
[56] E. N. Maslen, V. A. Sheltsov, N. R. Sheltsova, *Acta Crystallogr., Sect. B*, **1993**, *49*, 636, 980.
[57] J. Meister, W. H. E. Schwarz, *J. Phys. Chem*. **1994**, *98*, 8245.
[58] P. Seiler, *Acta Crystallogr.*, *Sect. B*, **1993**, *49*, 223.
[59] J. M. Savariault, M. S. Lehmann, *J. Am. Chem. Soc*. **1980**, *102*, 1298.
[60] Y. Wang, R. H. Blessing, F. K. Ross, P. Coppens, *Acta Cryst.*, *Sect. B*, **1976**, *32*, 572.
[61] F. L. Hirshfeld, *Acta Crystallogr., Sect B*, **1984**, *40*, 484.

[62] R. F. Stewart, *J. Chem. Phys.* **1969**, *51*, 4569.
[63] C. K. Johnson, 'ORTEP', USAEC Report No. ORNL-3794, 1965.
[64] E. Keller, SCHAKAL, Kristallographisches Institut, Universität Freiburg, Freiburg, Germany, 1990.
[65] K. Angermund, K. H. Claus, R. Goddard, C. Krüger (1985), *Angew. Chem.* **97**, 241; *Angew. Chem., Int. Ed. Eng.* **24**, 237.
[66] C. P. Brock, J. D. Dunitz, *Acta Crystallogr., Sect. B* **1990**, *46*, 795.
[67] J. D. Dunitz, W. B. Schweizer, P. Seiler, *Helv. Chim. Acta* **1983**, *66*, 123.
[68] J. D. Dunitz, P. Seiler, *Acta Crystallogr.*, *Sect. B* **1973**, *29*, 589.
[69] P. Seiler, W. B. Schweizer, J. D. Dunitz, *Acta Crystallogr.*, *Sect. B* **1984**, *40*, 319.
[70] B. Delley, *Chem. Phys.* **1986**, *110*, 329.
[71] H. Irngartinger, D. Kallfa, H. Prinzbach, O. Klingler, *Chem. Ber.* **1989**, *122*, 175.
[72] H. Neunhöffer, M. Clausen, H.-D. Vötter, H. Ohl, C. Krüger, K. Angermund, *Liebigs Ann. Chem.* **1985**, 1732.
[73] H. B. Bürgi, in 'Perspectives in Coordination Chemistry', Eds. A. F. Williams, C. Floriani, A. E. Merbach, Verlag Helvetica Chimica Acta, Basel, VCH, Weinheim, 1992, pp. 1 – 29.

Received April 5, 2001